

---

# Cause-Effect Inference in Location-Scale Noise Models: Maximum Likelihood vs. Independence Testing

---

Xiangyu Sun<sup>1</sup> Oliver Schulte<sup>1</sup>

## Abstract

Location-scale noise models (LSNMs) are a class of heteroscedastic structural causal models with wide applicability, closely related to affine flow models. Recent likelihood-based methods designed for LSNMs that infer cause-effect relationships achieve state-of-the-art accuracy, when their assumptions are satisfied concerning the noise distributions. However, under misspecification their accuracy deteriorates sharply, especially when the conditional variance in the anti-causal direction is smaller than that in the causal direction. In this paper, we demonstrate the misspecification problem and analyze why and when it occurs. We show that residual independence testing is much more robust to misspecification than likelihood-based cause-effect inference. Our empirical evaluation includes 580 synthetic and 99 real-world datasets.

## 1. Introduction

Distinguishing cause and effect is a fundamental problem in many disciplines, such as biology, healthcare and finance (Zhang & Chan, 2006; Huang, 2021; Mansouri et al., 2022). Randomized controlled trials (RCTs) are the gold standard for finding causal relationships. However, it may be unethical, expensive or even impossible to perform RCTs in real-world domains (Peters et al., 2017; Pearl & Mackenzie, 2018). Causal discovery algorithms aim to find causal relationships given observational data alone. Traditional causal discovery algorithms can only identify causal relationships up to Markov equivalence classes (MECs) (Spirtes & Glymour, 1991; Kalisch & Bühlman, 2007; Colombo et al., 2012). To break the symmetry in a MEC, additional assumptions are needed (Peters et al., 2017; Schölkopf, 2022), such as the type of functional dependence of effect on cause. Structural causal models (SCMs) specify a functional class for the causal relations in the data (Pearl, 2009; Peters et al., 2017). In this work, we focus on one particular type of SCM

called location-scale noise models (LSNMs) (Tagasovska et al., 2020; Khemakhem et al., 2021; Xu et al., 2022; Strobl & Lasko, 2022; Immer et al., 2022):

$$Y := f(X) + g(X) \cdot Z_Y \quad (1)$$

where  $X$  is the cause,  $Y$  is the effect, written  $X \rightarrow Y$ , and  $Z_Y$  is a latent noise variable independent of  $X$  (i.e.,  $X \perp\!\!\!\perp Z_Y$ ). The functions  $f$  and  $g$  are twice-differentiable on the domain of  $X$ , and  $g$  is strictly positive on the domain of  $X$ . LSNMs are closely related to affine flow models, where  $g(X) = \exp s(X)$  (Khemakhem et al., 2021). LSNMs generalize the widely studied additive noise models (ANMs, where  $g(x) = 1$  for all  $x$ ) and allow heteroscedasticity where the variance of  $Y$  conditional on  $X$ , (i.e.  $\mathbb{V}[Y|X]$ ) depends on the value of  $X$ .

Two major approaches for cause-effect inference in SCMs are maximum likelihood (ML) and independence testing (IT) of residuals vs. the (putative) cause (Mooij et al., 2016). Both have been recently evaluated for LSNMs (Khemakhem et al., 2021; Immer et al., 2022), with good accuracy, especially when the  $f$  and  $g$  functions are estimated by neural networks. Immer et al. note, however, that ML can be less robust than IT, in the sense that accuracy deteriorates when the noise distribution is not Gaussian.

In this paper we investigate the robustness of ML vs. IT. Our analysis shows that ML cause-effect inference performs poorly when two factors coincide: (1) *Noise Misspecification*: the ML method assumes a different noise distribution from the true one. (2) *Misleading Conditional Variances (CVs)*:  $\mathbb{V}[Y|X] > \mathbb{V}[X|Y]$  in the data generated by causal direction  $X \rightarrow Y$ . For example, in an experiment on synthetic datasets shown in Table 1 below, (i) changing the true noise distribution from Gaussian to uniform and (ii) manipulating the CV of effect  $Y$  given cause  $X$  (i.e.  $\mathbb{V}[Y|X]$ ), while keeping other settings equal, can decrease the rate of identifying the true causal direction from 100% to 10%. In contrast, IT approaches maintain a perfect 100% accuracy.

Both conditions (1) and (2) often hold in practice. For real-world domains, assumptions about the noise distribution can be hard to determine or verify. It is also common to have misleading CVs in real-world datasets. For example, in the Tübingen Cause-Effect Pairs Benchmark (Mooij et al.,

<sup>1</sup>Simon Fraser University, Burnaby, Canada. Correspondence to: Xiangyu Sun <xiangyu\_sun@sfu.ca>.

2016), about 40% of the real-world datasets exhibit a misleading CV (see Appendix Table 4).

We make the following contributions:

- Describe experiments and theoretical analysis to show that ML methods succeed when the noise distribution is known.
- Demonstrate empirically that ML methods often fail when the noise distribution is misspecified and CV is misleading.
- Introduce a new IT method based on an affine flow model.
- Demonstrate empirically that our IT method is robust to noise misspecification and misleading CVs.

The paper is structured as follows. We discuss related works and preliminaries in Sections 2 and 3, respectively. Section 4 examines when ML methods succeed and when they fail. Section 5 demonstrates the robustness of the IT approach. Evaluations on synthetic and real-world datasets are given in Section 6. The code and scripts to reproduce all the results can be found online <sup>1</sup>.

## 2. Related Works

*Causal Discovery.* Causal discovery methods have been well studied in machine learning (Spirtes & Glymour, 1991; Kalisch & Bühlman, 2007; Colombo et al., 2012). Assuming causal sufficiency (no latent confounders) and faithfulness, they find causal structure up to a MEC. To identify causal relations within a MEC, additional assumptions are needed (Peters et al., 2017; Schölkopf, 2022). SCMs exploit constraints that result from assumptions about the functional dependency of effects on causes. Functional dependencies are often studied in the fundamental case of two variables  $X$  and  $Y$ , the simplest MEC (Mooij et al., 2016). We follow this line of work and study two-variable LSNMs assuming causal sufficiency.

*Structural Causal Models.* Assuming a linear non-Gaussian acyclic model (LINGAM) (Shimizu et al., 2006), the causal direction was proved to be identifiable. The key idea in LINGAM is that in the true causal direction  $X \rightarrow Y$ , the model residuals are independent of  $X$ . We refer to methods derived from the LINGAM approach as *independence testing* (IT) methods. The more general additive noise model (ANM) (Hoyer et al., 2008) allows for nonlinear cause-effect relationships and is generally identifiable, except for some special cases. There are other identifiable SCMs, such as post-nonlinear models (Zhang & Hyvarinen, 2012) and Poisson generalized linear models (Park & Park, 2019).

*LSNM identifiability.* There are several identifiability results for the causal direction in LSNMs. Xu et al. (2022) prove LSNMs are identifiable for linear causal dependencies. Khemakhem et al. (2021) show that nonlinear LSNMs are identifiable with Gaussian noise. Strobl & Lasko (2022); Immer et al. (2022) prove LSNMs are identifiable except in some pathological cases (cf. Section 4.1).

*Cause-Effect Inference in LSNMs.* The blueprint is to fit two LSNM models for each direction  $X \rightarrow Y$  and  $X \leftarrow Y$  and select the direction with a higher model score. HECI (Xu et al., 2022) bins putative cause values and selects a direction based on a Bayesian information criterion based score. BQCD (Tagasovska et al., 2020) uses nonparametric quantile regression to approximate minimum description length to select the direction. GRCI (Strobl & Lasko, 2022) finds the direction based on mutual information between the putative cause and the model residuals. LOCI (Immer et al., 2022) models the conditional distribution of effect given cause with Gaussian natural parameters. Then, it chooses the direction based on either likelihood (LOCI-M) or independence (LOCI-H). CAREFL-M (Khemakhem et al., 2021) fits affine flow models and scores them by likelihood. CAREFL-M is more general than LOCI since LOCI uses a fixed Gaussian noise distribution prior, whereas CAREFL-M can utilize different prior distributions. We introduce CAREFL-H as a new IT method that scores the fitted affine flow models based on independence. DECI (Geffner et al., 2022) generalizes CAREFL-M to multivariate cases but is designed for ANMs. To our knowledge, the problem of misleading CVs is neither identified nor analyzed in previous work.

## 3. Preliminaries

In this section, we define the cause-effect inference problem and review the LSNM data likelihood.

### 3.1. Problem Definition: Cause-Effect Inference

Cause-effect inference takes as input a dataset  $D$  over two random variables  $X, Y$  with  $N$  observational data pairs  $(X, Y) = \{(x_1, y_1), (x_2, y_2), \dots, (x_N, y_N)\}$  generated by a ground-truth LSNM in Equation (1). The binary output decision indicates whether  $X$  causes  $Y$  ( $X \rightarrow Y$ ) or  $Y$  causes  $X$  ( $X \leftarrow Y$ ). We assume no latent confounders, selection bias or feedback cycles.

### 3.2. Definition of Maximum Likelihood Approach for LSNMs

An LSNM model for two variables  $(X, Y)$  is a pair  $(\rightarrow, P_Z)$ . The  $\rightarrow$  represents the direction  $X \rightarrow Y$  with parameter space  $f \equiv f_\theta, g \equiv g_\psi, P_X \equiv P_{X,\zeta}$ . The  $\leftarrow$  represents the direction  $X \leftarrow Y$  with parameter space  $h \equiv h_{\theta'}, k \equiv$

<sup>1</sup><https://github.com/xiangyu-sun-789/CAREFL-H>

$k_{\psi'}$ ,  $P_Y \equiv P_{Y,\zeta'}$ . For notational simplicity, we treat the model functions directly as model parameters and omit reference to their parameterizations. For example, we write  $f \equiv f_\theta$  for a function  $f$  that is implemented by a neural network with weights  $\theta$ . We refer to  $P_Z$  as the **model prior** noise distribution.

A parameterized LSNM model defines a data distribution as follows (Immer et al., 2022) (derivation in Appendix A):

$$\begin{aligned} & P_{\rightarrow, P_Z}(X, Y; f, g, P_X) \\ &= P_X(X) \cdot P_{Z_Y}\left(\frac{Y - f(X)}{g(X)}\right) \cdot \frac{1}{g(X)} \\ & P_{\leftarrow, P_Z}(X, Y; h, k, P_Y) \\ &= P_Y(Y) \cdot P_{Z_X}\left(\frac{X - h(Y)}{k(Y)}\right) \cdot \frac{1}{k(Y)} \end{aligned} \quad (2)$$

For conciseness, we use shorter notation  $P_{\rightarrow, P_Z}(X, Y)$  and  $P_{\leftarrow, P_Z}(X, Y)$  in later sections. The likelihood of a dataset  $D$  for a parametrized  $\rightarrow$  model is given by

$$P_{\rightarrow, P_Z}(D; f, g, P_X) = \prod_{i=1}^N P_{\rightarrow, P_Z}(x_i, y_i; f, g, P_X)$$

The ML approach estimates the ML parameters and utilizes them to score the  $\rightarrow$  model (similarly for the  $\leftarrow$  model):

$$\hat{f}, \hat{g}, \hat{P}_X := \arg \max_{f, g, P_X} P_{\rightarrow, P_Z}(D; f, g, P_X) \quad (3)$$

$$L_{\rightarrow, P_Z}(D) := P_{\rightarrow, P_Z}(D; \hat{f}, \hat{g}, \hat{P}_X) \quad (4)$$

## 4. Analysis of Maximum Likelihood Approach

In this section, we state existing and provide new identifiability results for LSNMs. We use theoretical analysis to understand why misspecified ML methods fail in the presence of misleading CVs (cf. Table 1).

### 4.1. Identifiability of LSNMs with Correct Noise Distribution

Strobl & Lasko (2022); Immer et al. (2022) prove the identifiability of LSNMs, assuming a correctly specified noise distribution. That is, given that the data generating distribution  $(X, Y)$  follows a LSNM in the direction  $X \rightarrow Y$ , the same distribution with equal likelihood cannot be induced by a LSNM in the backward direction  $X \leftarrow Y$ , except in some pathological cases. In terms of our notation, direction identifiability means that if  $(\rightarrow, P_Z)$  is the data generating model, then

$$P([L_{\rightarrow, P_Z}(D) - L_{\leftarrow, P_Z}(D)] > 0) \rightarrow 1 \text{ as } N \rightarrow \infty$$

Immer et al. prove the following identifiability result:

**Theorem 4.1** (Theorem 1 from (Immer et al., 2022)). *For data  $(X, Y)$  that follows a LSNM in both direction  $X \rightarrow Y$  and  $X \leftarrow Y$ , i.e.,*

$$\begin{aligned} Y &= f(X) + g(X) \cdot Z_Y, \text{ where } X \perp\!\!\!\perp Z_Y \\ X &= h(Y) + k(Y) \cdot Z_X, \text{ where } Y \perp\!\!\!\perp Z_X \end{aligned}$$

The following condition must be true:

$$\begin{aligned} & (\log p(y))'' + \frac{g'(x)}{G(x, y)} \cdot (\log p(y))' \\ & + \frac{\partial^2}{\partial y^2} \cdot \nu_{X|Y}(x|y) + \frac{g(x)}{G(x, y)} \cdot \frac{\partial^2}{\partial y \partial x} \cdot \nu_{X|Y}(x|y) \quad (5) \\ & + \frac{g'(x)}{G(x, y)} \cdot \frac{\partial}{\partial y} \cdot \nu_{X|Y}(x|y) = 0 \end{aligned}$$

where  $G(x, y) = g(x) \cdot f'(x) + g'(x) \cdot [y - f(x)] \neq 0$  and  $\nu_{X|Y}(x|y) = \log p_{Z_X}\left(\frac{x - h(y)}{k(y)}\right) - \log k(y)$ .

They state that Equation (5) will be false except for ‘‘pathological cases’’. In addition, Khemakhem et al. (2021) provide sufficient conditions for LSNMs with Gaussian noise to be identifiable. Our next theorem provides identifiability results for some non-Gaussian noise distributions:

**Theorem 4.2.** *Suppose that the true data-generating distribution follows an LSNM model in both  $X \rightarrow Y$  and  $X \leftarrow Y$  directions:*

1. *If the noise distribution is  $Uniform(a, b)$ , then both  $g(X)$  and  $k(Y)$  are constant functions.*
2. *If the noise distribution is  $ContinuousBernoulli(\lambda \neq 0.5)^2$  or  $Exponential(\lambda)$ , then one of the following conditions holds:*
  - *$g(X)^{-1}$  and  $k(Y)^{-1}$  are constant functions.*
  - *$g(X)^{-1}$  and  $k(Y)^{-1}$  are linear functions with the same coefficients on  $X$  and  $Y$ , respectively.*

The proof is in Appendix B. Essentially, the theorem shows that for Uniform, Exponential, and ContinuousBernoulli noise distributions, the true LSNM model can be identified unless it degenerates to (i) a homoscedastic additive noise model or (ii) a heteroscedastic model with the same linear scale in both directions.

### 4.2. Non-Identifiability of LSNMs with Misspecified Noise Distribution

Existing identifiability results for ML methods require knowing the ground-truth noise distribution. We find that when

<sup>2</sup>The case of  $ContinuousBernoulli(\lambda = 0.5)$  is equivalent to  $Uniform(0, 1)$ .

Table 1: **Accuracy** over 10 datasets generated by SCM **LSNM-sine-tanh** (definition in Appendix G) with  $N = 10,000$  samples. The task is a binary decision whether  $X$  causes  $Y$  or  $Y$  causes  $X$ . Rewrite Equation (1) as  $Y = f(X) + \alpha \cdot g(X) \cdot Z_Y$ , where  $\alpha$  is a scale factor to alter the CV. CVs are computed by binning the putative cause.  $X$  denotes the ground-truth cause and  $Y$  denotes the ground-truth effect. We used  $Gaussian(0, 1)$  as model noise prior for both CAREFL and LOCI. The suffix  $-M$  denotes a ML method. The suffix  $-H$  denotes the corresponding IT method (more in Section 5).

True Noise	$Gaussian(0, 1)$					$Uniform(-1, 1)$				
	$\alpha$	0.1	0.5	1	5	10	0.1	0.5	1	5
$\bar{\mathbb{V}}[Y X]$	0.166	0.615	0.834	0.990	0.997	0.044	0.404	0.673	0.975	0.994
vs.	vs.	vs.	vs.	vs.	vs.	vs.	vs.	vs.	vs.	vs.
$\bar{\mathbb{V}}[X Y]$	0.455	0.709	0.793	0.821	0.817	0.047	0.375	0.566	0.681	0.677
CAREFL-M	1.0	1.0	1.0	1.0	1.0	0.7	0.6	0.7	0.1	0.1
LOCI-M	1.0	1.0	1.0	1.0	1.0	0.7	0.6	0.7	0.1	0.1
CAREFL-H	1.0	1.0	1.0	1.0	1.0	0.9	1.0	1.0	1.0	1.0
LOCI-H	1.0	1.0	1.0	1.0	1.0	0.7	1.0	1.0	1.0	1.0

the noise distribution is misspecified for both causal and anti-causal models, the anti-causal model may achieve a higher data likelihood, even in the sample size limit. In other words, ML model selection is not consistent when the noise distribution is misspecified. In terms of our notation, if  $(\rightarrow, P_Z)$  is the data generating model, but the noise distribution is misspecified as  $P'_Z$ , then

$$P([L_{\rightarrow, P'_Z}(D) - L_{\leftarrow, P'_Z}(D)] > 0) \not\rightarrow 1 \text{ as } N \rightarrow \infty$$

We conducted a simple experiment to show that with a misspecified noise distribution, ML model selection can fail badly. Table 1 shows results for CAREFL-M (Khemakhem et al., 2021) and LOCI-M (Immer et al., 2022) with model prior distribution  $Gaussian(0, 1)$ . For the left half of the table, the data was generated with  $Gaussian(0, 1)$  noise, matching the model specification. In this case, both CAREFL-M and LOCI-M work quite well, and increasing CV in the causal direction does not affect their accuracy. For the right half of the table, the data was generated with  $Uniform(-1, 1)$  noise, contradicting the model specification. With the misspecified noise, the accuracy of both CAREFL-M and LOCI-M decreases to 70%. With both misspecified noise and misleading CVs, their accuracy becomes even lower. For example, in the last column when  $\bar{\mathbb{V}}[Y|X] = 0.994$  and  $\bar{\mathbb{V}}[X|Y] = 0.677$ , both CAREFL-M and LOCI-M give an accuracy of just 10%. Thus they select the incorrect anti-causal direction 9 out of 10 times.

To understand why higher CV corresponds to lower data likelihood, note that the model Equation (2) entails the following relationships for the  $X \rightarrow Y$  model:

$$\begin{aligned} \mathbb{V}[Y|X] &= g^2(X) \cdot \mathbb{V}[Z_Y] \\ P_{\rightarrow, P_Z}(X, Y) &= P_X(X) \cdot P_{Z_Y}(Z_Y) \cdot \frac{1}{g(X)} \end{aligned}$$

where  $Z_Y = \frac{Y-f(X)}{g(X)}$ . Therefore we can expect  $\mathbb{V}[Y|X]$  and  $P_{\rightarrow, P_Z}(X, Y)$  to be negatively related:

1. Increasing  $\mathbb{V}[Y|X]$  by enlarging  $g(X)$  reduces  $\frac{1}{g(X)}$ , which in turn reduces  $P_{\rightarrow, P_Z}(X, Y)$ .
2. High variance typically means small densities. Therefore, increasing  $\mathbb{V}[Y|X]$  by enlarging  $\mathbb{V}[Z_Y]$  often reduces  $P_{Z_Y}(Z_Y)$ , which in turn reduces  $P_{\rightarrow, P_Z}(X, Y)$ .

Figure 1 illustrates these relationships in actual datasets.

1. CV and likelihood are negatively related (Figures 1a and 1b), with correctly or incorrectly specified noise.
2. When the noise distribution is correctly specified, the causal model always has a higher likelihood, even with misleading CVs (Figure 1a).
3. When the noise distribution is misspecified, the anti-causal model often has a higher likelihood under misleading CVs (Figure 1b).

## 5. Robustness of Independence Testing

This section describes IT approaches for cause-effect learning in LSNMs, including a new IT method based on affine flows. A theoretical analysis explains why IT approaches are robust to noise misspecification and misleading CVs.

### 5.1. The Independence Testing Approach

Inspired by the breakthrough LINGAM approach, independence testing has been used in existing methods for various SCMs (Hoyer et al., 2008; Shimizu et al., 2011; Peters et al., 2014; Strobl & Lasko, 2022; Immer et al., 2022). Like the

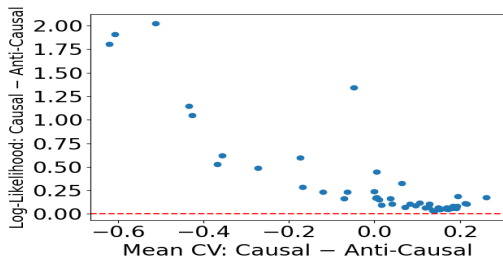
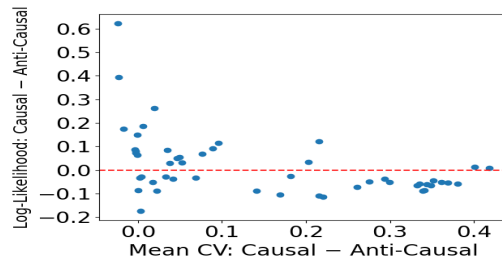
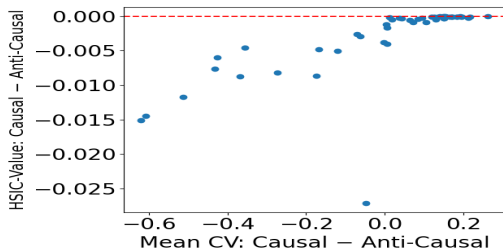
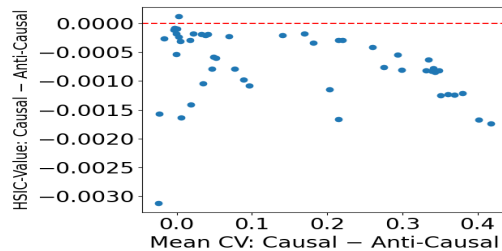
(a) Log-Likelihood Difference Under Correct Noise Specification:  $Gaussian(0, 1)$  noise(b) Log-Likelihood Difference Under Noise Misspecification:  $Uniform(-1, 1)$  noise(c) HSIC Difference Under Correct Noise Specification:  $Gaussian(0, 1)$  noise(d) HSIC Difference Under Noise Misspecification:  $Uniform(-1, 1)$  noise

Figure 1: Visualization of Table 1. First row (1a,1b): ML methods. Second row (1c,1d): IT methods.  $Y\text{-axis} < 0.0$ : A ML method returns the *incorrect* anti-causal direction.  $Y\text{-axis} > 0.0$ : An IT method returns the *incorrect* anti-causal direction. ML methods may fail under misspecification and misleading CVs (1b). IT methods are more robust (1d).

ML approach (Equation (4)), IT methods fit the model parameters in both directions, typically maximizing the data likelihood (Equation (3)). The difference is in the model selection step: While ML approaches select the direction with the highest likelihood, IT approaches select the direction with the highest degree of independence between the fitted model residuals and the putative cause. Algorithm 1 provides pseudo-code.

As in previous work (e.g., Mooij et al. (2016)), we use the Hilbert-Schmidt independence criterion (HSIC) (Gretton et al., 2005) to measure (in)dependence throughout the paper. HSIC measures the squared distance between the joint probability of the two variables and the product of their marginals embedded in the reproducible kernel Hilbert space. We have  $HSIC(U, V) = 0$  if and only if  $U \perp\!\!\!\perp V$ .

To fit the functions in a LSNM, we use the affine flow estimator  $\mathbf{T}$  from CAREFL-M (Khemakhem et al., 2021). We refer to the resulting IT method as **CAREFL-H**. This combination of affine flow with IT appears to be new. Details on CAREFL-M and learning the flow transformation  $\mathbf{T}$  are given in Appendix C.

Another approach to IT methods is to test the independence of residuals for both  $X$  and  $Y$  variables (He et al., 2021). We found that this performs similarly to CAREFL-H and therefore report experimental results only for the more common LINGAM-style approach. More details on IT with

residuals are in Appendix D.

## 5.2. Suitability Theory

With a consistent HSIC estimator, Mooij et al. (2016) show that an IT approach consistently selects the causal direction for ANMs if *the regression method is suitable*. A regression method is suitable if the expected mean squared error between the predicted residuals  $\hat{E}$  and the true residuals  $E$  approaches 0 in the limit of  $N \rightarrow \infty$ :

$$\lim_{N \rightarrow \infty} \mathbb{E}_{D, D'} \left[ \frac{1}{N} \|\hat{E}_{1 \dots N} - E_{1 \dots N}\|^2 \right] = 0 \quad (6)$$

where  $D$  and  $D'$  denote training set and testing set, respectively. Hence, with enough data a suitable regression method reconstructs the ground-truth noise.

If an HSIC estimator is consistent, the estimated HSIC value converges in probability to the population HSIC value.

$$\widehat{HSIC}(X, Y) \xrightarrow{P} HSIC(X, Y).$$

Mooij et al. (2016) show that even a biased HSIC estimator with a fixed bounded kernel is consistent.

With a consistent HSIC estimator and a suitable regression method, the consistency result for ANMs in Mooij et al. (2016) extends naturally to LSNMs.

**Proposition 5.1.** *For identifiable LSNMs with an independent noise term in one causal direction only, if an IT ap-*

**Algorithm 1** CAREFL-H

- 
- 1: **Input:** data pairs  $D := (X, Y)$ , the flow estimator  $\mathbf{T}$  of CAREFL-M with prior  $P_Z$ , and an HSIC estimator
  - 2: **Output:** estimated causal direction  $dir$
  - 3: Split  $D$  into training set  $D_{train} := (X_{train}, Y_{train})$  and testing set  $D_{test} := (X_{test}, Y_{test})$
  - 4: Optimize  $\mathbf{T}_{\hat{\theta}, \hat{\psi}, \hat{\zeta}}(D_{train}; P_Z)$  in  $X \rightarrow Y$  direction via ML to estimate  $\hat{f}$  and  $\hat{g}$
  - 5: Compute the residual  $\hat{Z}_Y := \frac{Y_{test} - \hat{f}(X_{test})}{\hat{g}(X_{test})}$
  - 6: Optimize  $\mathbf{T}_{\hat{\theta}', \hat{\psi}', \hat{\zeta}'}(D_{train}; P_Z)$  in  $X \leftarrow Y$  direction via ML to estimate  $\hat{h}$  and  $\hat{k}$
  - 7: Compute the residual  $\hat{Z}_X := \frac{X_{test} - \hat{h}(Y_{test})}{\hat{k}(Y_{test})}$
  - 8: **if**  $HSIC(X_{test}, \hat{Z}_Y) < HSIC(Y_{test}, \hat{Z}_X)$  **then**
  - 9:      $dir := X \rightarrow Y$
  - 10: **else if**  $HSIC(X_{test}, \hat{Z}_Y) > HSIC(Y_{test}, \hat{Z}_X)$  **then**
  - 11:      $dir := X \leftarrow Y$
  - 12: **else**
  - 13:      $dir := no\ conclusion$
  - 14: **end if**
- 

*proach is used with a suitable regression method for LSNMs and a consistent HSIC estimator, then the IT approach is consistent for inferring causal direction for LSNMs.*

### 5.3. Suitability: Empirical Results

The *suitability value*  $S$  is the left-hand side of Equation (6). Table 2 shows an empirical evaluation of  $S$  for the flow estimator  $\mathbf{T}$  in the causal direction. We generate data from 3 synthetic LSNMs (definition in Appendix G), and evaluate  $\mathbf{T}$  under noise misspecification and misleading CVs. We find that as the sample size grows,  $S$  approaches 0. In other words,  $\mathbf{T}$  is *empirically suitable under noise misspecification and misleading CVs*. Therefore, according to Proposition 5.1, CAREFL-H based on the flow estimator  $\mathbf{T}$  and a consistent HSIC estimator is empirically consistent for inferring causal direction in LSNMs under noise misspecification and misleading CVs.

Because the  $\mathbf{T}$  in CAREFL-M (Khemakhem et al., 2021) uses neural networks to approximate the observed data distribution, it is difficult to provide a theoretical guarantee of suitability. Therefore, although our experiments indicate that  $\mathbf{T}$  is often suitable in practice, we do not claim that it is suitable for all LSNMs. For example, we have found it to be not suitable in the low-noise regime when the LSNMs are close to deterministic.

## 6. Experiments

The code and scripts to reproduce all the results are given online<sup>3</sup>. We show that across hyperparameter choices the IT approach (i.e., CAREFL-H) produces much higher accuracy than the ML approach (i.e., CAREFL-M) in the difficult settings with noise misspecification and misleading CVs, and produces comparable accuracy in the easier settings without noise misspecification or misleading CVs. Also the IT approach is more robust with real-world data, where the ground-truth noise distribution is unknown.

For all experiments, we start with the same default hyperparameter values for both CAREFL-M and CAREFL-H and alter one hyperparameter value at a time. The default hyperparameter values are those specified in CAREFL-M (Khemakhem et al., 2021) for the Tübingen Cause-Effect Pairs Benchmark (Mooij et al., 2016). Please see Appendix F for more details on default and alternative hyperparameter values. Previous work (Mooij et al., 2016; Immer et al., 2022) reported that ML methods perform better with data splitting (split data into training set for model fitting and testing set for model selection) and IT methods perform better with data recycling (the same data is used for both model fitting and selection). Therefore, we use both splitting methods: (i) CAREFL(0.8): 80% as training and 20% as testing. (ii) CAREFL(1.0): training = testing = 100%.

We use a consistent HSIC estimator with Gaussian kernels (Pfister et al., 2018). A summary of experimental datasets is provided in Appendix Table 4. All the datasets are normalized to have mean 0 and variance 1.

### 6.1. Synthetic Datasets

Please see Appendix G for the definition of the 3 ground-truth LSNM SCMs and details on how synthetic datasets are generated from them. The sample sizes in each synthetic dataset are 500 or 5,000. As shown in Appendix Table 4, most synthetic datasets generated by such SCMs have misleading CVs. Based on the analysis of Section 4.2 we formulate the following hypotheses. (i) We expect CAREFL-M to be accurate given a correct noise specification with or without misleading CVs. (ii) With noise misspecification but without misleading CVs, we expect the accuracy of CAREFL-M to be reduced. (iii) With both noise misspecification and misleading CVs, we expect the accuracy to be very low, often below 50%. Overall, the results from the experiments confirm our hypotheses.

#### 6.1.1. NOISE MISSPECIFICATION

We evaluate CAREFL-M and CAREFL-H against data generated with  $Uniform(-1, 1)$ ,  $Exponential(1)$ ,

<sup>3</sup><https://github.com/xiangyu-sun-789/CAREFL-H>

Table 2: Suitability of the flow estimator  $\mathbf{T}$  of CAREFL-M in the causal direction under noise misspecification and misleading CVs.  $\mathbf{T}$  is trained with a Laplace prior. The original dataset with size  $2N$  is split into two: 50% as training set and 50% as testing set.  $\bar{\mathbb{V}}[Y|X] > \bar{\mathbb{V}}[X|Y]$  indicates misleading CVs in the dataset.

	N=50	N=500	N=1000	N=5000
(a) <b>LSNM-tanh-exp-cosine</b> and <b>ContinuousBernoulli(0.9)</b> noise. $\bar{\mathbb{V}}[Y X]$ vs. $\bar{\mathbb{V}}[X Y]$ : 0.324 vs. 0.291.	$[S_{Z_1}, S_{Z_2}]$   [0.02406, 0.01283]	[0.00194, 0.00204]	[0.00094, 0.00092]	[0.0002, 0.00018]
(b) <b>LSNM-sine-tanh</b> and <b>Uniform(-1, 1)</b> noise. $\bar{\mathbb{V}}[Y X]$ vs. $\bar{\mathbb{V}}[X Y]$ : 0.422 vs. 0.367.	$[S_{Z_1}, S_{Z_2}]$   [0.0081, 0.00285]	[0.00039, 0.00031]	[0.0002, 0.00017]	[0.00003, 0.00003]
(c) <b>LSNM-sigmoid-sigmoid</b> and <b>Exponential(1)</b> noise. $\bar{\mathbb{V}}[Y X]$ vs. $\bar{\mathbb{V}}[X Y]$ : 0.927 vs. 0.657.	$[S_{Z_1}, S_{Z_2}]$   [0.00979, 0.00443]	[0.00074, 0.00058]	[0.00045, 0.00026]	[0.00005, 0.00005]

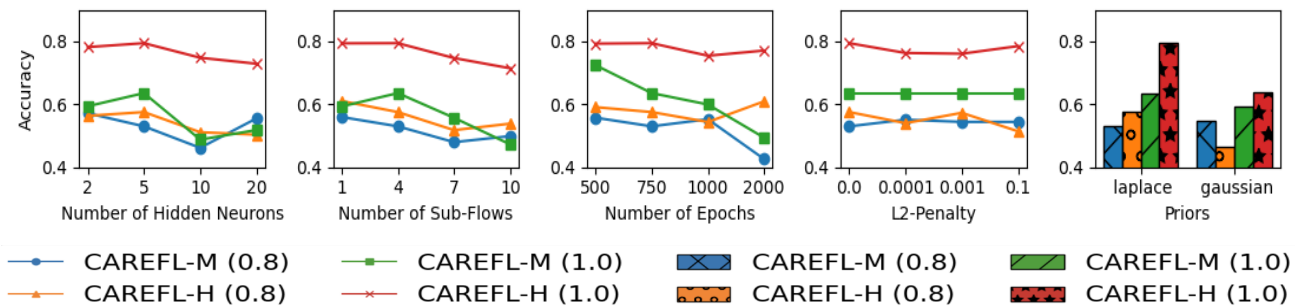


Figure 2: **Weighted accuracy** over 99 datasets from **Tübingen Cause-Effect Pairs Benchmark**.

*ContinuousBernoulli(0.9)* or *Beta(0.5, 0.5)* noise, covered by our identifiability Theorem 4.2 (except *Beta(0.5, 0.5)*). Khemakhem et al. (2021) claim that CAREFL-M is robust to noise misspecification. We show that it may fail remarkably.

We summarize findings from the 336 settings here; the detailed results are given in Appendix Figures 3 to 14. In 289 settings (86.01%), both CAREFL-M(0.8) and CAREFL-M(1.0) select the correct causal direction with less than 50% random accuracy. Furthermore, in 110 settings (32.74%) both CAREFL-M(0.8) and CAREFL-M(1.0) fail catastrophically with an accuracy of 0%. These experiments also show that the accuracy of CAREFL-M often decreases as  $N$  increases. In contrast, CAREFL-H(1.0) achieves better accuracy than CAREFL-M in 333 settings (99.11%). The accuracy of CAREFL-H(1.0) goes below 50% in only 6 settings (1.79%). The results demonstrate the robustness of the IT approach under noise misspecification and misleading CVs, across different hyperparameter choices.

Appendix Table 4 and Appendix Figure 14 show that with misleading CVs, the accuracy of CAREFL-M is close to 0%.

This is much lower than the corresponding cases without misleading CVs in Appendix Figures 6 and 10.

### 6.1.2. CORRECT NOISE SPECIFICATION

These experiments show that CAREFL-H is comparable with CAREFL-M under correct noise specification, with or without misleading CVs, especially on larger datasets, as long as the affine model capacity is sufficient. We evaluate CAREFL-M and CAREFL-H against data generated with *Gaussian(0, 1)* and *Laplace(0, 1)* noise. The detailed results are in Appendix Figures 15 to 20. We find that CAREFL-M is more sample efficient than CAREFL-H when the model prior matches the data. Consistent with the suitability results in Section 5.3, the accuracy of CAREFL-H improves with more data. For example, with  $N = 500$ , there are 49 out of 84 settings (58.33%) where CAREFL-M outperforms CAREFL-H(1.0). However, with  $N = 5,000$ , CAREFL-H(1.0) achieves similar accuracy as CAREFL-M on all datasets (except LSNM-sigmoid-sigmoid with *Laplace(0, 1)* noise.) In addition, CAREFL-H(1.0) may underperform CAREFL-M when the number of hidden neu-

Table 3: The best accuracy of each method on the SIM and Tübingen Cause-Effect Pairs benchmarks. For methods other than CAREFL-M and CAREFL-H, we use the results reported in Immer et al. (2022).

(a) SIM Benchmarks

	LOCI-M	LOCI-H	GRCI	BQCD	HECI	CAM	RESIT	CAREFL-M	CAREFL-H
SIM	0.53	0.79	0.77	0.62	0.49	0.57	0.77	0.55	<b>0.80</b>
SIM-c	0.50	0.83	0.77	0.72	0.55	0.60	0.82	0.58	<b>0.85</b>
SIM-ln	0.79	0.72	0.77	0.80	0.65	<b>0.87</b>	<b>0.87</b>	0.84	0.83
SIM-G	0.78	<b>0.82</b>	0.70	0.64	0.56	0.81	0.78	<b>0.82</b>	0.79

(b) Weighted Accuracy for Tübingen Cause-Effect Pairs Benchmark

	LOCI-M	LOCI-H	GRCI	BQCD	HECI	CAM	RESIT	CAREFL-M	CAREFL-H
Tübingen Cause-Effect Pairs	0.57	0.64	<b>0.82</b>	0.77	0.71	0.58	0.57	0.73	<b>0.82</b>

rons, sub-flows or training epochs is low. The reason is that an IT approach requires more power to fit the LSNM functions and produce a good reconstruction of the noise.

## 6.2. Synthetic Benchmark

Similar to Tagasovska et al. (2020); Immer et al. (2022), we compare CAREFL-M and CAREFL-H against the SIM benchmark suite (Mooij et al., 2016). SIM comprises 4 sub-benchmarks: default (SIM), with one confounder (SIM-c), low noise levels (SIM-ln) and Gaussian noise (SIM-G). In this benchmark, most datasets do not have misleading CVs (Appendix Table 4), which favors ML methods. Each sub-benchmark contains 100 datasets and each dataset has  $N = 1000$  data pairs. As shown in Appendix Figure 21, CAREFL-M and CAREFL-H(1.0) achieve similar accuracy on SIM-ln and SIM-G across different hyperparameter choices. For SIM and SIM-c, CAREFL-H, especially CAREFL-H(1.0), outperforms CAREFL-M by 20%-30% in all settings. The accuracy of CAREFL-M is only about random guess (40%-60%) on SIM and SIM-c.

Table 3a compares CAREFL-H with SOTA methods. For each CAREFL method, we report the best accuracy obtained with the hyperparameter settings considered in Appendix Figure 21, without further tuning. CAREFL-H achieves the best accuracy on SIM and SIM-c, and achieves competitive accuracy on SIM-ln and SIM-G.

## 6.3. Real-World Benchmark: Tübingen Cause-Effect

We compare CAREFL-M and CAREFL-H against real-world datasets from the Tübingen Cause-Effect Pairs Benchmark (Mooij et al., 2016). The benchmark is commonly used to evaluate cause-effect inference algorithms (Khemakhem et al., 2021; Xu et al., 2022; Immer et al., 2022).

To be consistent with previous work (Tagasovska et al., 2020; Strobl & Lasko, 2022; Immer et al., 2022), we exclude 6 multivariate and 3 discrete datasets (#47, #52-#55, #70, #71, #105, #107) and utilize the remaining 99 bivariate datasets. As recommended by Mooij et al. (2016), we report weighted accuracy. 40% of datasets in the benchmark feature misleading CVs. As shown in Figure 2, CAREFL-H(1.0) outperforms CAREFL-M in all configurations by large margins (7%-30%).

We also compare CAREFL-H with SOTA methods. Following Khemakhem et al. (2021), we use a single set of hyperparameters for all 99 datasets, found by grid search (Appendix H). Table 3b shows that CAREFL-H achieves the SOTA accuracy (82%). With the respectively best hyperparameter settings, CAREFL-H is 9% more accurate than CAREFL-M (Khemakhem et al., 2021).

## 7. Conclusion and Future Work

We identified a failure of maximum-likelihood (ML) methods for cause-effect inference in location-scale noise models. Our analysis shows that the failure mode occurs when the noise distribution is misspecified and conditional effect variances are misleading (i.e., higher in the causal direction). Selecting causal models by independence tests (IT) is robust even in this difficult setting. Extensive empirical evaluation compared the ML approach and a new IT method based on affine flows, using both synthetic and real-world datasets. The IT flow method achieves better accuracy under noise misspecification and misleading CVs, with robust performance across different hyperparameter choices. Future directions include improving the sample efficiency of IT methods, and improving the robustness of ML methods by learning the noise distribution instead of using a fixed prior.

## References

- Colombo, D., Maathuis, M. H., Kalisch, M., and Richardson, T. S. Learning high-dimensional directed acyclic graphs with latent and selection variables. *The Annals of Statistics*, pp. 294–321, 2012.
- Geffner, T., Antoran, J., Foster, A., Gong, W., Ma, C., Kiciman, E., Sharma, A., Lamb, A., Kukla, M., Pawlowski, N., et al. Deep end-to-end causal inference. *arXiv preprint arXiv:2202.02195*, 2022.
- Gretton, A., Bousquet, O., Smola, A., and Schölkopf, B. Measuring statistical dependence with hilbert-schmidt norms. In *International conference on algorithmic learning theory*, pp. 63–77. Springer, 2005.
- He, Y., Cui, P., Shen, Z., Xu, R., Liu, F., and Jiang, Y. Daring: Differentiable causal discovery with residual independence. In *Proceedings of the 27th ACM SIGKDD Conference on Knowledge Discovery & Data Mining*, pp. 596–605, 2021.
- Hoyer, P., Janzing, D., Mooij, J. M., Peters, J., and Schölkopf, B. Nonlinear causal discovery with additive noise models. *Advances in neural information processing systems*, 21, 2008.
- Huang, B. Diagnosis of autism spectrum disorder by causal influence strength learned from resting-state fmri data. In *Neural Engineering Techniques for Autism Spectrum Disorder*, pp. 237–267. Elsevier, 2021.
- Immer, A., Schultheiss, C., Vogt, J. E., Schölkopf, B., Bühlmann, P., and Marx, A. On the identifiability and estimation of causal location-scale noise models. *arXiv preprint arXiv:2210.09054*, 2022.
- Kalisch, M. and Bühlmann, P. Estimating high-dimensional directed acyclic graphs with the pc-algorithm. *Journal of Machine Learning Research*, 8(3), 2007.
- Khemakhem, I., Monti, R., Leech, R., and Hyvarinen, A. Causal autoregressive flows. In *International conference on artificial intelligence and statistics*, pp. 3520–3528. PMLR, 2021.
- Kingma, D. P. and Ba, J. Adam: A method for stochastic optimization. *arXiv preprint arXiv:1412.6980*, 2014.
- Mansouri, M., Khakabimamaghani, S., Chindelevitch, L., and Ester, M. Aristotle: stratified causal discovery for omics data. *BMC bioinformatics*, 23(1):1–18, 2022.
- Mooij, J. M., Peters, J., Janzing, D., Zscheischler, J., and Schölkopf, B. Distinguishing cause from effect using observational data: methods and benchmarks. *The Journal of Machine Learning Research*, 17(1):1103–1204, 2016.
- Park, G. and Park, S. High-dimensional poisson structural equation model learning via  $\ell_1$ -regularized regression. *J. Mach. Learn. Res.*, 20:95–1, 2019.
- Pearl, J. *Causality*. Cambridge university press, 2009.
- Pearl, J. and Mackenzie, D. *The book of why: the new science of cause and effect*. Basic books, 2018.
- Peters, J., Mooij, J. M., Janzing, D., and Schölkopf, B. Causal discovery with continuous additive noise models. 2014.
- Peters, J., Janzing, D., and Schölkopf, B. *Elements of causal inference: foundations and learning algorithms*. The MIT Press, 2017.
- Pfister, N., Bühlmann, P., Schölkopf, B., and Peters, J. Kernel-based tests for joint independence. *Journal of the Royal Statistical Society: Series B (Statistical Methodology)*, 80(1):5–31, 2018.
- Schölkopf, B. Causality for machine learning. In *Probabilistic and Causal Inference: The Works of Judea Pearl*, pp. 765–804. 2022.
- Shimizu, S., Hoyer, P. O., Hyvärinen, A., Kerminen, A., and Jordan, M. A linear non-gaussian acyclic model for causal discovery. *Journal of Machine Learning Research*, 7(10), 2006.
- Shimizu, S., Inazumi, T., Sogawa, Y., Hyvarinen, A., Kawahara, Y., Washio, T., Hoyer, P. O., Bollen, K., and Hoyer, P. Directlingam: A direct method for learning a linear non-gaussian structural equation model. *Journal of Machine Learning Research-JMLR*, 12(Apr):1225–1248, 2011.
- Spirites, P. and Glymour, C. An algorithm for fast recovery of sparse causal graphs. *Social science computer review*, 9(1):62–72, 1991.
- Strobl, E. V. and Lasko, T. A. Identifying patient-specific root causes with the heteroscedastic noise model. *arXiv preprint arXiv:2205.13085*, 2022.
- Tagasovska, N., Chavez-Demoulin, V., and Vatter, T. Distinguishing cause from effect using quantiles: Bivariate quantile causal discovery. In *International Conference on Machine Learning*, pp. 9311–9323. PMLR, 2020.
- Xu, S., Mian, O. A., Marx, A., and Vreeken, J. Inferring cause and effect in the presence of heteroscedastic noise. In *International Conference on Machine Learning*, pp. 24615–24630. PMLR, 2022.
- Zhang, K. and Chan, L.-W. Extensions of ica for causality discovery in the hong kong stock market. In *International Conference on Neural Information Processing*, pp. 400–409. Springer, 2006.

Zhang, K. and Hyvarinen, A. On the identifiability of the post-nonlinear causal model. *arXiv preprint arXiv:1205.2599*, 2012.

Zheng, X., Aragam, B., Ravikumar, P. K., and Xing, E. P. Dags with no tears: Continuous optimization for structure learning. *Advances in Neural Information Processing Systems*, 31, 2018.

Zheng, X., Dan, C., Aragam, B., Ravikumar, P., and Xing, E. Learning sparse nonparametric dags. In *International Conference on Artificial Intelligence and Statistics*, pp. 3414–3425. PMLR, 2020.

## A. Derivation of Equation (2)

**Lemma A.1.** For a LSNM model  $X \rightarrow Y$  defined in Equation (1), we have  $P_{Y|X}(Y|X) = P_{Z_Y}(\frac{Y-f(X)}{g(X)}) \cdot \frac{1}{g(X)}$ , where  $P_{Z_Y}$  is the noise distribution.

For the data distribution in the  $X \rightarrow Y$  direction:

$$P_{\rightarrow, P_Z}(X, Y) = P_X(X) \cdot P_{Y|X}(Y|X) = P_X(X) \cdot P_{Z_Y}(\frac{Y-f(X)}{g(X)}) \cdot \frac{1}{g(X)}$$

Similarly, in the  $X \leftarrow Y$  direction:

$$P_{\leftarrow, P_Z}(X, Y) = P_Y(Y) \cdot P_{X|Y}(X|Y) = P_Y(Y) \cdot P_{Z_X}(\frac{X-h(Y)}{k(Y)}) \cdot \frac{1}{k(Y)}$$

*Proof for Lemma A.1.* For a LSNM model defined in Equation (1), we have  $Z_Y = \frac{Y-f(X)}{g(X)}$ . Hence,  $\frac{\partial Z_Y}{\partial Y} = \frac{1}{g(X)}$ . Since  $g(X) > 0$ , so  $|\frac{\partial Z_Y}{\partial Y}| = |\frac{1}{g(X)}| = \frac{1}{g(X)}$ .

$$\begin{aligned} & P_{Y|X}(Y|X) \\ &= P_{Z_Y}(Z_Y|X) \cdot |\det \frac{\partial Z_Y}{\partial Y}| \\ & \quad (\text{via change of variables}) \\ &= P_{Z_Y}(Z_Y) \cdot |\det \frac{\partial Z_Y}{\partial Y}| \\ &= P_{Z_Y}(\frac{Y-f(X)}{g(X)}) \cdot |\frac{\partial Z_Y}{\partial Y}| \\ &= P_{Z_Y}(\frac{Y-f(X)}{g(X)}) \cdot \frac{1}{g(X)} \end{aligned}$$

□

## B. Identifiability Proofs

In this section, we prove Theorem 4.2.

If the data  $(x, y)$  follows a LSNM in the forward (i.e. causal) model:

$$y := f(x) + g(x) \cdot z_Y$$

where  $z_X$  and  $z_Y$  are the noise terms,  $e \perp\!\!\!\perp z_X$ ,  $x \perp\!\!\!\perp z_Y$ ,  $g(x) > 0$  for all  $x$  on its domain. We assume  $f(\cdot)$  and  $g(\cdot)$  are twice-differentiable on the domain of  $x$ .

If the data  $(x, y)$  follows a LSNM in the backward (i.e. anti-causal) model:

$$x := h(y) + k(y) \cdot m_X$$

where  $m_Y$  and  $m_X$  are the noise terms,  $e' \perp\!\!\!\perp m_Y$ ,  $y \perp\!\!\!\perp m_X$ ,  $k(y) > 0$  for all  $y$  on its domain. We assume  $h(\cdot)$  and  $k(\cdot)$  are twice-differentiable on the domain of  $y$ .

$z_X, z_Y, m_Y$  and  $m_X$  follow one of *Uniform*( $a, b$ ), *Exponential*( $\lambda$ ) or *ContinuousBernoulli*( $\lambda$ ) distribution accordingly.

*Proof for Uniform*( $a, b$ ) *Noise.* For the causal model, according to Lemma A.1, we have  $P_{Y|X}(y|x) = P_{Z_Y}(\frac{y-f(x)}{g(x)}) \cdot \frac{1}{g(x)} = P_{Z_Y}(z_Y) \cdot \frac{1}{g(x)} = \frac{1}{b-a} \cdot \frac{1}{g(x)} = \frac{1}{(b-a) \cdot g(x)}$ . Similarly, for the backward model, we have  $P_{X|Y}(x|y) = \frac{1}{(b-a) \cdot k(y)}$ .

The joint likelihood of the observation  $(x, y)$  in the causal model is:

$$P_{\rightarrow, P_Z}(x, y) = P_X(x) \cdot P_{Y|X}(y|x) = P_X(x) \cdot \frac{1}{(b-a) \cdot g(x)}$$

The joint likelihood of the observation  $(x, y)$  in the backward model is:

$$P_{\leftarrow, P_Z}(x, y) = P_Y(y) \cdot P_{X|Y}(x|y) = P_Y(y) \cdot \frac{1}{(b-a) \cdot k(y)}$$

If the data follows both models:

$$\begin{aligned} P_{\rightarrow, P_Z}(x, y) &= P_{\leftarrow, P_Z}(x, y) \\ P_X(x) \cdot \frac{1}{(b-a) \cdot g(x)} &= P_Y(y) \cdot \frac{1}{(b-a) \cdot k(y)} \\ P_X(x) \cdot \frac{1}{g(x)} &= P_Y(y) \cdot \frac{1}{k(y)} \end{aligned}$$

Take the derivative of both sides with respect to  $x$ :

$$\begin{aligned} P_X(x) \cdot (g(x)^{-1})' + (P_X(x))' \cdot g(x)^{-1} &= 0 \\ P_X(x) \cdot -1 \cdot g(x)^{-2} \cdot g(x)' + 0 \cdot g(x)^{-1} &= 0 \\ P_X(x) \cdot -1 \cdot g(x)^{-2} \cdot g(x)' &= 0 \\ P_X(x) &> 0 \\ g(x)^{-2} = \frac{1}{g(x)^2} &> 0 \\ \text{Therefore, } g(x)' &= 0 \end{aligned}$$

Similarly, if we take the derivative of both sides with respect to  $y$  instead, we have:

$$k(y)' = 0$$

These imply that both  $g(x)$  and  $k(y)$  are constant functions. □

*Proof for Exponential( $\lambda$ ) Noise.* For the causal model, according to Lemma A.1, we have  $P_{Y|X}(y|x) = P_{Z_Y}(\frac{y-f(x)}{g(x)}) \cdot \frac{1}{g(x)} = \lambda \cdot e^{-\lambda \cdot \frac{y-f(x)}{g(x)}} \cdot \frac{1}{g(x)} = \frac{\lambda}{g(x)} \cdot e^{-\frac{\lambda}{g(x)} \cdot (y-f(x))}$ . Similarly, for the backward model, we have  $P_{X|Y}(x|y) = \frac{\lambda}{k(y)} \cdot e^{-\frac{\lambda}{k(y)} \cdot (x-h(y))}$ .

The joint likelihood of the observation  $(x, y)$  in the causal model is:

$$\begin{aligned} P_{\rightarrow, P_Z}(x, y) &= P_X(x) \cdot P_{Y|X}(y|x) = P_X(x) \cdot \frac{\lambda}{g(x)} \cdot e^{-\frac{\lambda}{g(x)} \cdot (y-f(x))} \\ \log P_{\rightarrow, P_Z}(x, y) &= \log P_X(x) + \log \lambda - \log g(x) - \frac{\lambda}{g(x)} \cdot (y-f(x)) \end{aligned}$$

The joint likelihood of the observation  $(x, y)$  in the backward model is:

$$\begin{aligned} P_{\leftarrow, P_Z}(x, y) &= P_Y(y) \cdot P_{X|Y}(x|y) = P_Y(y) \cdot \frac{\lambda}{k(y)} \cdot e^{-\frac{\lambda}{k(y)} \cdot (x-h(y))} \\ \log P_{\leftarrow, P_Z}(x, y) &= \log P_Y(y) + \log \lambda - \log k(y) - \frac{\lambda}{k(y)} \cdot (x-h(y)) \end{aligned}$$

If the data follows both models:

$$\begin{aligned}
 \log P_{\rightarrow, P_Z}(x, y) &= \log P_{\leftarrow, P_Z}(x, y) \\
 \log P_X(x) + \log \lambda - \log g(x) - \frac{\lambda}{g(x)} \cdot (y - f(x)) \\
 &= \log P_Y(y) + \log \lambda - \log k(y) - \frac{\lambda}{k(y)} \cdot (x - h(y)) \\
 \log P_X(x) - \log g(x) - \lambda \cdot g(x)^{-1} \cdot y + \lambda \cdot g(x)^{-1} \cdot f(x) \\
 &= \log P_Y(y) - \log k(y) - \lambda \cdot k(y)^{-1} \cdot x + \lambda \cdot k(y)^{-1} \cdot h(y)
 \end{aligned}$$

Take the derivative of both sides with respect to  $x$ :

$$\begin{aligned}
 (\log P_X(x))' - (\log g(x))' - \lambda \cdot y \cdot (g(x)^{-1})' + \lambda \cdot (g(x)^{-1})' \cdot f(x) \\
 = -\lambda \cdot k(y)^{-1}
 \end{aligned}$$

Take the derivative of both sides with respect to  $y$ :

$$\begin{aligned}
 -\lambda \cdot (g(x)^{-1})' &= -\lambda \cdot (k(y)^{-1})' \\
 \frac{\partial g(x)^{-1}}{\partial x} &= \frac{\partial k(y)^{-1}}{\partial y}
 \end{aligned}$$

They can be equal only if both sides are constants. Therefore,  $g(x)^{-1}$  and  $k(y)^{-1}$  are both constants or both linear functions with the same coefficient on  $x$  and  $y$ , respectively.  $\square$

*Proof for ContinuousBernoulli* ( $\lambda \neq 0.5$ ) *Noise*. Please refer to *Uniform* for *ContinuousBernoulli* ( $\lambda = 0.5$ ), which equals to *Uniform*(0, 1). For the causal model, according to Lemma A.1, we have  $P_{Y|X}(y|x) = P_{Z_Y}(\frac{y-f(x)}{g(x)}) \cdot \frac{1}{g(x)} = C_\lambda \cdot \lambda^{\frac{y-f(x)}{g(x)}} \cdot (1-\lambda)^{1-\frac{y-f(x)}{g(x)}} \cdot \frac{1}{g(x)}$ , where  $C_\lambda$  is the normalizing constant of the continuous Bernoulli distribution. Similarly, for the backward model, we have  $P_{X|Y}(x|y) = C_\lambda \cdot \lambda^{\frac{x-h(y)}{k(y)}} \cdot (1-\lambda)^{1-\frac{x-h(y)}{k(y)}} \cdot \frac{1}{k(y)}$ .

The joint likelihood of the observation  $(x, y)$  in the causal model is:

$$\begin{aligned}
 P_{\rightarrow, P_Z}(x, y) &= P_X(x) \cdot P_{Y|X}(y|x) = P_X(x) \cdot \frac{1}{g(x)} \cdot C_\lambda \cdot \lambda^{\frac{y-f(x)}{g(x)}} \\
 &\quad \cdot (1-\lambda)^{1-\frac{y-f(x)}{g(x)}} \\
 \log P_{\rightarrow, P_Z}(x, y) &= \log P_X(x) - \log g(x) + \log C_\lambda + \log \lambda^{\frac{y-f(x)}{g(x)}} \\
 &\quad + \log(1-\lambda)^{1-\frac{y-f(x)}{g(x)}}
 \end{aligned}$$

The joint likelihood of the observation  $(x, y)$  in the backward model is:

$$\begin{aligned}
 P_{\leftarrow, P_Z}(x, y) &= P_Y(y) \cdot P_{X|Y}(x|y) = P_Y(y) \cdot \frac{1}{k(y)} \cdot C_\lambda \cdot \lambda^{\frac{x-h(y)}{k(y)}} \\
 &\quad \cdot (1-\lambda)^{1-\frac{x-h(y)}{k(y)}} \\
 \log P_{\leftarrow, P_Z}(x, y) &= \log P_Y(y) - \log k(y) + \log C_\lambda + \log \lambda^{\frac{x-h(y)}{k(y)}} \\
 &\quad + \log(1-\lambda)^{1-\frac{x-h(y)}{k(y)}}
 \end{aligned}$$

If the data follows both models:

$$\begin{aligned}
 & \log P_{\rightarrow, P_Z}(x, y) = \log P_{\leftarrow, P_Z}(x, y) \\
 & \log P_X(x) - \log g(x) + \log C_\lambda + \log \lambda^{\frac{y-f(x)}{g(x)}} + \log(1-\lambda)^{1-\frac{y-f(x)}{g(x)}} \\
 = & \log P_Y(y) - \log k(y) + \log C_\lambda + \log \lambda^{\frac{x-h(y)}{k(y)}} + \log(1-\lambda)^{1-\frac{x-h(y)}{k(y)}} \\
 & \log P_X(x) - \log g(x) + \log C_\lambda + \frac{y-f(x)}{g(x)} \cdot \log \lambda + \left(1 - \frac{y-f(x)}{g(x)}\right) \\
 & \cdot \log(1-\lambda) \\
 = & \log P_Y(y) - \log k(y) + \log C_\lambda + \frac{x-h(y)}{k(y)} \cdot \log \lambda + \left(1 - \frac{x-h(y)}{k(y)}\right) \\
 & \cdot \log(1-\lambda) \\
 & \log P_X(x) - \log g(x) + \log C_\lambda + g(x)^{-1} \cdot \log \lambda \cdot y - g(x)^{-1} \cdot \\
 & \log \lambda \cdot f(x) + \log(1-\lambda) - \log(1-\lambda) \cdot g(x)^{-1} \cdot y + \log(1-\lambda) \cdot g(x)^{-1} \cdot f(x) \\
 = & \log P_Y(y) - \log k(y) + \log C_\lambda + k(y)^{-1} \cdot \log \lambda \cdot x - k(y)^{-1} \cdot \\
 & \log \lambda \cdot h(y) + \log(1-\lambda) - \log(1-\lambda) \cdot k(y)^{-1} \cdot x + \log(1-\lambda) \cdot k(y)^{-1} \cdot h(y)
 \end{aligned}$$

Take the derivative of both sides with respect to  $x$ :

$$\begin{aligned}
 & (\log P_X(x))' - g(x)^{-1} \cdot g(x)' - 1 \cdot g(x)^{-2} \cdot g(x)' \cdot \log \lambda \cdot y \\
 & - (g(x)^{-1} \cdot \log \lambda \cdot f(x))' - \log(1-\lambda) \cdot -1 \cdot g(x)^{-2} \cdot g(x)' \cdot y \\
 & + (\log(1-\lambda) \cdot g(x)^{-1} \cdot f(x))' = k(y)^{-1} \cdot \log \lambda - \log(1-\lambda) \cdot k(y)^{-1}
 \end{aligned}$$

Take the derivative of both sides with respect to  $y$ :

$$\begin{aligned}
 & -g(x)^{-2} \cdot g(x)' \cdot \log \lambda - \log(1-\lambda) \cdot -1 \cdot g(x)^{-2} \cdot g(x)' \\
 = & -1 \cdot k(y)^{-2} \cdot k(y)' \cdot \log \lambda - \log(1-\lambda) \cdot -1 \cdot k(y)^{-2} \cdot k(y)' \\
 & g(x)^{-2} \cdot g(x)' \cdot \log \lambda - \log(1-\lambda) \cdot g(x)^{-2} \cdot g(x)' \\
 = & k(y)^{-2} \cdot k(y)' \cdot \log \lambda - \log(1-\lambda) \cdot k(y)^{-2} \cdot k(y)' \\
 & g(x)^{-2} \cdot g(x)' \cdot (\log \lambda - \log(1-\lambda)) = k(y)^{-2} \cdot k(y)' \cdot (\log \lambda - \log(1-\lambda)) \\
 & \text{Since } \lambda \neq 0.5, \text{ therefore } \log \lambda - \log(1-\lambda) \neq 0 \\
 & g(x)^{-2} \cdot g(x)' = k(y)^{-2} \cdot k(y)' \\
 & \frac{\partial g(x)^{-1}}{\partial x} = \frac{\partial k(y)^{-1}}{\partial y}
 \end{aligned}$$

They can be equal only if both sides are constants. Therefore,  $g(x)^{-1}$  and  $k(y)^{-1}$  are both constants or both linear functions with the same coefficient on  $x$  and  $y$ , respectively.  $\square$

### C. CAREFL-M

CAREFL-M (Khemakhem et al., 2021) models a LSNM in Equation (1) via affine flows  $\mathbf{T}$ . Each sub-flow  $T_k \in \mathbf{T}$  is defined as the following:

$$\begin{aligned}
 X &= t_1 + e^{s_1} \cdot Z_X \\
 Y &= t_2(X) + e^{s_2(X)} \cdot Z_Y
 \end{aligned} \tag{7}$$

where  $X$  is the putative cause and  $Y$  is the putative effect in  $X \rightarrow Y$  direction.  $t_1$  and  $s_1$  are constants.  $t_2$  and  $s_2$  are functions parameterized using neural networks. Without loss of generality,  $X$  is assumed to be a function of latent noise

**Algorithm 2** CAREFL-M

- 1: **Input:** data pairs  $D := (X, Y)$ , and the flow estimator  $\mathbf{T}$  with prior  $P_Z$
- 2: **Output:** estimated causal direction  $dir$
- 3: Split  $D$  into training set  $D_{train} := (X_{train}, Y_{train})$  and testing set  $D_{test} := (X_{test}, Y_{test})$
- 4: Optimize  $\mathbf{T}_{\hat{t}_1, \hat{s}_1, \hat{t}_2, \hat{s}_2}(D_{train}; P_Z)$  in  $X \rightarrow Y$  direction via ML
- 5: Compute the likelihood  $\hat{L}_{\rightarrow, P_Z}(D_{test}; \mathbf{T}_{\hat{t}_1, \hat{s}_1, \hat{t}_2, \hat{s}_2})$  in  $X \rightarrow Y$  direction
- 6: Optimize  $\mathbf{T}_{\hat{t}'_1, \hat{s}'_1, \hat{t}'_2, \hat{s}'_2}(D_{train}; P_Z)$  in  $X \leftarrow Y$  direction via ML
- 7: Compute the likelihood  $\hat{L}_{\leftarrow, P_Z}(D_{test}; \mathbf{T}_{\hat{t}'_1, \hat{s}'_1, \hat{t}'_2, \hat{s}'_2})$  in  $X \leftarrow Y$  direction
- 8: **if**  $\hat{L}_{\rightarrow, P_Z}(D_{test}; \mathbf{T}_{\hat{t}_1, \hat{s}_1, \hat{t}_2, \hat{s}_2}) > \hat{L}_{\leftarrow, P_Z}(D_{test}; \mathbf{T}_{\hat{t}'_1, \hat{s}'_1, \hat{t}'_2, \hat{s}'_2})$  **then**
- 9:      $dir := X \rightarrow Y$
- 10: **else if**  $\hat{L}_{\rightarrow, P_Z}(D_{test}; \mathbf{T}_{\hat{t}_1, \hat{s}_1, \hat{t}_2, \hat{s}_2}) < \hat{L}_{\leftarrow, P_Z}(D_{test}; \mathbf{T}_{\hat{t}'_1, \hat{s}'_1, \hat{t}'_2, \hat{s}'_2})$  **then**
- 11:      $dir := X \leftarrow Y$
- 12: **else**
- 13:      $dir := no\ conclusion$
- 14: **end if**

variable  $Z_X$ . If  $t_1 = 0$  and  $s_1 = 0$ , then  $X = Z_X$ . The exponential function  $e$  ensures the multipliers to  $Z$  are positive without expression loss. Similarly, for the backward direction  $X \leftarrow Y$ :

$$\begin{aligned} Y &= t'_1 + e^{s'_1} \cdot Z_Y \\ X &= t'_2(Y) + e^{s'_2(Y)} \cdot Z_X \end{aligned} \quad (8)$$

where  $Y$  is the putative cause and  $X$  is the putative effect in  $X \leftarrow Y$  direction.  $t'_1$  and  $s'_1$  are constants.  $t'_2$  and  $s'_2$  are functions parameterized using neural networks.

Given Equation (7), the joint log-likelihood of  $(x, y)$  in  $X \rightarrow Y$  direction is:

$$\log P_{\rightarrow, P_Z}(x, y) = \log P_{Z_X}(e^{-s_1} \cdot (x - t_1)) + \log P_{Z_Y}(e^{-s_2(x)} \cdot (y - t_2(x))) - s_1 - s_2(x) \quad (9)$$

Similarly for the  $X \leftarrow Y$  direction. Note that the priors  $P_Z = \{P_{Z_X}, P_{Z_Y}\}$  in Equation (9) may mismatch the unknown ground-truth noise distribution  $P_Z^* = \{P_{Z_X}^*, P_{Z_Y}^*\}$ . Both CAREFL-M and CAREFL-H optimizes Equation (9) for each direction over the training set. For CAREFL-M, it chooses the direction with ML Score  $L$  over the testing set as the estimated causal direction. Detailed procedure for CAREFL-M is given in Algorithm 2. To map the parameters  $\theta, \psi, \zeta, \theta', \psi'$  and  $\zeta'$  in LSNM (Equation (2)) to the flow estimator  $\mathbf{T}$  of CAREFL (Equations (7) and (8)), we have  $f_\theta \equiv t_2, g_\psi \equiv e^{s_2}, P_{X, \zeta} \equiv \{t_1, e^{s_1}\}, f_{\theta'} \equiv t'_2, g_{\psi'} \equiv e^{s'_2}$  and  $P_{Y, \zeta'} \equiv \{t'_1, e^{s'_1}\}$ .

## D. CAREFL-H Alternative Independence Testing

In Algorithm 1, CAREFL-H tests independence between the putative cause and the residual of the putative effect in each direction, i.e., between  $X$  and  $\hat{Z}_Y$  in  $X \rightarrow Y$  direction, and between  $Y$  and  $\hat{Z}_X$  in  $X \leftarrow Y$  direction. An alternative way of testing independence is to test between the residual of the putative cause and the residual of the putative effect (He et al., 2021), i.e., between  $\hat{Z}_X$  and  $\hat{Z}_Y$  in both directions. Please see Algorithm 3 for complete steps.

**Theorem D.1.** *By optimizing the log-likelihood in the causal direction, may or may not under noise misspecification, CAREFL-H gives the reconstructed residual of the ground-truth cause (i.e.  $\hat{Z}_X$ ) identical to the ground-truth cause (i.e.  $X$ ) and to the latent noise variable of the cause (i.e.  $Z_X$ ) up to shifting and scaling.*

Proof is in Appendix E. Although we prove only for the cause, empirically we find that in the causal direction the reconstructed residual of the ground-truth effect (i.e.,  $\hat{Z}_Y$ ) is also close to the latent noise variable of the effect (i.e.,  $Z_Y$ ). According to Theorem D.1, testing  $HSIC(X, \hat{Z}_Y)$  in Algorithm 1 and  $HSIC(\hat{Z}_X, \hat{Z}_Y)$  in Algorithm 3 for the causal direction are equivalent. The difference comes from testing  $HSIC(Y, \hat{Z}_X)$  in Algorithm 1 and  $HSIC(\hat{Z}_X, \hat{Z}_Y)$  in Algorithm 3 for the anti-causal direction. Although in our experiments the two algorithms often produce the same estimation of causal direction, we prefer Algorithm 1, since it relies on few estimations of the residuals.

**Algorithm 3** CAREFL-H (Between Residuals)

- 1: **Input:** data pairs  $D := (X, Y)$ , the flow estimator  $\mathbf{T}$  of CAREFL-M with prior  $P_Z$ , and an HSIC estimator
- 2: **Output:** estimated causal direction  $dir$
- 3: Split  $D$  into training set  $D_{train} := (X_{train}, Y_{train})$  and testing set  $D_{test} := (X_{test}, Y_{test})$
- 4: Optimize  $\mathbf{T}_{\hat{t}_1, \hat{s}_1, \hat{t}_2, \hat{s}_2}(D_{train}; P_Z)$  in  $X \rightarrow Y$  direction via ML to estimate  $\hat{t}_1, \hat{s}_1, \hat{t}_2$  and  $\hat{s}_2$
- 5: Compute the residuals  $\hat{Z}_{X, \rightarrow} := \frac{X_{test} - \hat{t}_1}{e^{\hat{s}_1}}$  and  $\hat{Z}_{Y, \rightarrow} := \frac{Y_{test} - \hat{t}_2(X)}{e^{\hat{s}_2(X)}}$
- 6: Optimize  $\mathbf{T}_{\hat{t}'_1, \hat{s}'_1, \hat{t}'_2, \hat{s}'_2}(D_{train}; P_Z)$  in  $X \leftarrow Y$  direction via ML to estimate  $\hat{t}'_1, \hat{s}'_1, \hat{t}'_2$  and  $\hat{s}'_2$
- 7: Compute the residuals  $\hat{Z}_{Y, \leftarrow} := \frac{Y_{test} - \hat{t}'_1}{e^{\hat{s}'_1}}$  and  $\hat{Z}_{X, \leftarrow} := \frac{X_{test} - \hat{t}'_2(Y)}{e^{\hat{s}'_2(Y)}}$
- 8: **if**  $HSIC(\hat{Z}_{X, \rightarrow}, \hat{Z}_{Y, \rightarrow}) < HSIC(\hat{Z}_{X, \leftarrow}, \hat{Z}_{Y, \leftarrow})$  **then**
- 9:      $dir := X \rightarrow Y$
- 10: **else if**  $HSIC(\hat{Z}_{X, \rightarrow}, \hat{Z}_{Y, \rightarrow}) > HSIC(\hat{Z}_{X, \leftarrow}, \hat{Z}_{Y, \leftarrow})$  **then**
- 11:      $dir := X \leftarrow Y$
- 12: **else**
- 13:      $dir := no\ conclusion$
- 14: **end if**

**E. Proof for Theorem D.1**

In this section, we prove Theorem D.1.

The flow estimator  $\mathbf{T}$  in CAREFL-M (Khemakhem et al., 2021) models a LSNM in Equation (1) as the following:

$$\begin{aligned} X &= t_1 + e^{s_1} \cdot Z_X \\ Y &= t_2(X) + e^{s_2(X)} \cdot Z_Y \end{aligned} \tag{10}$$

where  $X$  and  $Y$  are putative cause and effect, respectively.  $Z_X$  and  $Z_Y$  are assumed to follow a prior distribution, e.g.  $Gaussian(0, 1)$  or  $Laplace(0, 1)$ .  $t_1$  and  $s_1$  are constants. It also means  $Z_X$  is identical to  $X$  up to shifting and scaling. If  $t_1 = 0$  and  $s_1 = 0$ , then  $X = Z_X$ .  $t_2$  and  $s_2$  are functions parameterized using neural networks. Let  $(x^n, y^n)$ , where  $n \in \{1, \dots, N\}$ , be the  $n$ -th data pair.

Fact 1, invert Equation (10):

$$\begin{aligned} z_X^n &= e^{-s_1} \cdot (x^n - t_1) \\ z_Y^n &= e^{-s_2(x^n)} \cdot (y^n - t_2(x^n)) \end{aligned}$$

Fact 2, how  $\hat{z}_X^n$  and  $\hat{z}_Y^n$  are computed in the flow estimator  $\mathbf{T}$ :

$$\begin{aligned} \hat{z}_X^n &= e^{-\hat{s}_1} \cdot (x^n - \hat{t}_1) \\ \hat{z}_Y^n &= e^{-\hat{s}_2(x^n)} \cdot (y^n - \hat{t}_2(x^n)) \end{aligned}$$

Fact 3, how the flow estimator  $\mathbf{T}$  is trained via ML (may under noise misspecification):

$$\begin{aligned}
 p_X(x^n, y^n) &= p_{Z_X}(\widehat{z}_X^n) \cdot p_{Z_Y}(\widehat{z}_Y^n) \cdot \left| \det \begin{bmatrix} \frac{\partial \widehat{z}_X^n}{\partial x^n} & \frac{\partial \widehat{z}_X^n}{\partial y^n} \\ \frac{\partial \widehat{z}_Y^n}{\partial x^n} & \frac{\partial \widehat{z}_Y^n}{\partial y^n} \end{bmatrix} \right| \\
 &= p_{Z_X}(e^{-\widehat{s}_1} \cdot (x^n - \widehat{t}_1)) \cdot p_{Z_Y}(e^{-\widehat{s}_2(x^n)} \cdot (y^n - \widehat{t}_2(x^n))) \\
 &\cdot \left| \det \begin{bmatrix} e^{-\widehat{s}_1} & 0 \\ \frac{\partial \widehat{z}_Y^n}{\partial x^n} & e^{-\widehat{s}_2(x^n)} \end{bmatrix} \right| \\
 &= p_{Z_X}(e^{-\widehat{s}_1} \cdot (x^n - \widehat{t}_1)) \cdot p_{Z_Y}(e^{-\widehat{s}_2(x^n)} \cdot (y^n - \widehat{t}_2(x^n))) \\
 &\cdot |e^{-\widehat{s}_1} \cdot e^{-\widehat{s}_2(x^n)} - 0| \\
 &= p_{Z_X}(e^{-\widehat{s}_1} \cdot (x^n - \widehat{t}_1)) \cdot p_{Z_Y}(e^{-\widehat{s}_2(x^n)} \cdot (y^n - \widehat{t}_2(x^n))) \cdot e^{-\widehat{s}_1} \cdot e^{-\widehat{s}_2(x^n)} \\
 &= p_{Z_X}(e^{-\widehat{s}_1} \cdot (e^{s_1} \cdot z_X^n + t_1 - \widehat{t}_1)) \\
 &\cdot p_{Z_Y}(e^{-\widehat{s}_2(x^n)} \cdot (e^{s_2(x^n)} \cdot z_Y^n + t_2(x^n) - \widehat{t}_2(x^n))) \\
 &\cdot e^{-\widehat{s}_1} \cdot e^{-\widehat{s}_2(x^n)} \\
 &= p_{Z_X}(e^{-\widehat{s}_1} \cdot (e^{s_1} \cdot z_X^n + t_1 - \widehat{t}_1)) \cdot e^{-\widehat{s}_1} \\
 &\cdot p_{Z_Y}(e^{-\widehat{s}_2(x^n)} \cdot (e^{s_2(x^n)} \cdot z_Y^n + t_2(x^n) - \widehat{t}_2(x^n))) \cdot e^{-\widehat{s}_2(x^n)} \\
 &= p_{Z_X}(e^{s_1 - \widehat{s}_1} \cdot z_X^n + e^{-\widehat{s}_1} \cdot (t_1 - \widehat{t}_1)) \cdot e^{-\widehat{s}_1} \\
 &\cdot p_{Z_Y}(e^{s_2(x^n) - \widehat{s}_2(x^n)} \cdot z_Y^n + e^{-\widehat{s}_2(x^n)} \cdot (t_2(x^n) - \widehat{t}_2(x^n))) \cdot e^{-\widehat{s}_2(x^n)}
 \end{aligned}$$

Assume the priors  $p_{Z_X}$  and  $p_{Z_Y}$  are standard Gaussian  $N(0, 1)$  for math convenience. The proof is analogous with other prior distributions, e.g., standard Laplace. We do not make assumptions on the ground-truth noise distribution, which allows noise misspecification.

$$\begin{aligned}
 p_X(x^n, y^n) &= N(e^{s_1 - \widehat{s}_1} \cdot z_X^n + e^{-\widehat{s}_1} \cdot (t_1 - \widehat{t}_1); \mu = 0, \sigma^2 = 1) \cdot e^{-\widehat{s}_1} \\
 &\cdot N(e^{s_2(x^n) - \widehat{s}_2(x^n)} \cdot z_Y^n + e^{-\widehat{s}_2(x^n)} \cdot (t_2(x^n) - \widehat{t}_2(x^n)); \mu = 0, \sigma^2 = 1) \\
 &\cdot e^{-\widehat{s}_2(x^n)} \\
 &\text{(the PDF of } N(x; 0, 1) \text{ is } \frac{1}{\sqrt{2\pi}} \cdot e^{-\frac{1}{2} \cdot (x)^2}) \\
 &= \frac{1}{\sqrt{2\pi}} \cdot e^{-\frac{1}{2} \cdot (e^{s_1 - \widehat{s}_1} \cdot z_X^n + e^{-\widehat{s}_1} \cdot (t_1 - \widehat{t}_1))^2} \cdot e^{-\widehat{s}_1} \\
 &\cdot \frac{1}{\sqrt{2\pi}} \cdot e^{-\frac{1}{2} \cdot (e^{s_2(x^n) - \widehat{s}_2(x^n)} \cdot z_Y^n + e^{-\widehat{s}_2(x^n)} \cdot (t_2(x^n) - \widehat{t}_2(x^n)))^2} \cdot e^{-\widehat{s}_2(x^n)} \\
 \ln p_X(x^n, y^n) &= \ln \frac{1}{\sqrt{2\pi}} - \frac{1}{2} \cdot (e^{s_1 - \widehat{s}_1} \cdot z_X^n + e^{-\widehat{s}_1} \cdot (t_1 - \widehat{t}_1))^2 - \widehat{s}_1 \\
 &+ \ln \frac{1}{\sqrt{2\pi}} - \frac{1}{2} \cdot (e^{s_2(x^n) - \widehat{s}_2(x^n)} \cdot z_Y^n + e^{-\widehat{s}_2(x^n)} \cdot (t_2(x^n) - \widehat{t}_2(x^n)))^2 \\
 &- \widehat{s}_2(x^n)
 \end{aligned}$$

**Lemma E.1.** To maximize the log-likelihood, may or may not under noise misspecification,  $\widehat{t}_1 = E[X]$ , a constant.

**Lemma E.2.** To maximize the log-likelihood, may or may not under noise misspecification,  $\widehat{s}_1 = E[\ln |\widehat{t}_1 - X|]$ , a constant.

$$\begin{aligned}
 \widehat{z}_X^n &= e^{-\widehat{s}_1} \cdot (x^n - \widehat{t}_1) \\
 \widehat{z}_X^n &= e^{-E[\ln |\widehat{t}_1 - X|]} \cdot (x^n - \widehat{t}_1) \\
 \widehat{z}_X^n &= e^{-E[\ln |E[X] - X|]} \cdot (x^n - E[X]) \\
 \widehat{z}_X^n &= C_1 \cdot (x^n - C_2)
 \end{aligned}$$

Therefore,  $\widehat{Z}_X$  and  $X$  are identically distributed up to shifting and scaling.

Since  $x^n := t_1 + e^{s_1} \cdot z_X^n$ , we have:

$$\begin{aligned}\widehat{z}_X^n &= C_1 \cdot (x^n - C_2) \\ &= C_1 \cdot (e^{s_1} \cdot z_X^n + t_1 - C_2) \\ &= C_1 \cdot e^{s_1} \cdot z_X^n + C_1 \cdot t_1 - C_1 \cdot C_2 \\ &= C_3 \cdot z_X^n + C_4 - C_5 \\ &= C_3 \cdot z_X^n + C_6\end{aligned}$$

Therefore,  $\widehat{Z}_X$  and  $Z_X$  are also identically distributed up to shifting and scaling.

*Proof for Lemma E.1.*

$$\frac{\partial \ln p_X(x^n, y^n)}{\partial \widehat{t}_1} = e^{-\widehat{s}_1} \cdot (z_X^n \cdot e^{s_1 - \widehat{s}_1} + e^{-\widehat{s}_1} \cdot (t_1 - \widehat{t}_1))$$

$$\begin{aligned}\text{Let } e^{-\widehat{s}_1} \cdot (z_X^n \cdot e^{s_1 - \widehat{s}_1} + e^{-\widehat{s}_1} \cdot (t_1 - \widehat{t}_1)) &= 0 \\ \widehat{t}_1 &= t_1 + z_X^n \cdot e^{s_1} = x^n\end{aligned}$$

Similarly, for  $\frac{\partial \ln p_X(x^{n-1}, y^{n-1})}{\partial \widehat{t}_1}$ ,  $\widehat{t}_1 = x^{n-1}$ ; for  $\frac{\partial \ln p_X(x^{n-2}, y^{n-2})}{\partial \widehat{t}_1}$ ,  $\widehat{t}_1 = x^{n-2}$ . Therefore,

$$\widehat{t}_1 = \frac{1}{n} \cdot \sum_{n=1}^N x^n = E[X]$$

Since  $\frac{\partial^2 \ln p_X(x^n, y^n)}{\partial^2 \widehat{t}_1}$  is negative,  $\widehat{t}_1$  maximizes the log-likelihood. □

*Proof for Lemma E.2.*

$$\frac{\partial \ln p_X(x^n, y^n)}{\partial \widehat{s}_1} = (-z_X^n \cdot e^{s_1 - \widehat{s}_1} - (t_1 - \widehat{t}_1) \cdot e^{-\widehat{s}_1})^2 - 1$$

$$\begin{aligned}\text{Let } (-z_X^n \cdot e^{s_1 - \widehat{s}_1} - (t_1 - \widehat{t}_1) \cdot e^{-\widehat{s}_1})^2 - 1 &= 0 \\ \pm e^{\widehat{s}_1} &= \widehat{t}_1 - x^n \\ e^{\widehat{s}_1} &= \pm(\widehat{t}_1 - x^n) \\ e^{\cdot} &\text{ must be positive.} \\ e^{\widehat{s}_1} &= |\widehat{t}_1 - x^n| \\ \widehat{s}_1 &= \ln |\widehat{t}_1 - x^n|\end{aligned}$$

Similarly, for  $\frac{\partial \ln p_X(x^{n-1}, y^{n-1})}{\partial \widehat{s}_1}$ ,  $\widehat{s}_1 = \ln |\widehat{t}_1 - x^{n-1}|$ ; for  $\frac{\partial \ln p_X(x^{n-2}, y^{n-2})}{\partial \widehat{s}_1}$ ,  $\widehat{s}_1 = \ln |\widehat{t}_1 - x^{n-2}|$ . Therefore,

$$\widehat{s}_1 = \frac{1}{n} \cdot \sum_{n=1}^N \ln |\widehat{t}_1 - x^n| = E[\ln |\widehat{t}_1 - X|]$$

Since  $\frac{\partial^2 \ln p_X(x^n, y^n)}{\partial^2 \widehat{s}_1}$  is negative,  $\widehat{s}_1$  maximizes the log-likelihood. □

## F. Default and Alternative Hyperparameter Values Used in Section 6

We use the reported hyperparameter values in CAREFL-M (Khemakhem et al., 2021) for the Tübingen Cause-Effect Pairs Benchmark (Mooij et al., 2016) as the default hyperparameter values in all our experiments:

- The flow estimator  $\mathbf{T}$  is parameterized with 4 sub-flows (alternatively: 1, 7 and 10).
- For each sub-flow,  $f$ ,  $g$ ,  $h$  and  $k$  are modelled as four-layer MLPs with 5 hidden neurons in each layer (alternatively: 2, 10 and 20).
- Prior distribution is Laplace (alternatively: Gaussian prior).
- Adam optimizer (Kingma & Ba, 2014) is used to train each model for 750 epochs (alternatively: 500, 1000 and 2000).
- L2-penalty strength is 0 by default (alternatively: 0.0001, 0.001, 0.1).

Although we also observe that LOCI-H is more robust than LOCI-M under noise misspecification and misleading CVs, we omit their results because: (1) CAREFL often outperforms LOCI (see Tables 1 and 3). (2) LOCI is fixed as a Gaussian distribution, whereas CAREFL can specify different prior distributions. (3) For conciseness. LOCI uses different set of hyperparameters than CAREFL. So their results cannot be merged into the same figures.

## G. Synthetic SCMs Used in Section 6.1

We use the following SCMs to generate synthetic datasets:

- LSNM-tanh-exp-cosine:  $Y := \tanh(X \cdot \theta_1) \cdot \theta_2 + e^{\cos(X \cdot \psi_1) \cdot \psi_2} \cdot Z_Y$
- LSNM-sine-tanh:  $Y := \sin(X \cdot \theta_1) \cdot \theta_2 + (\tanh(X \cdot \psi) + \phi) \cdot Z_Y$
- LSNM-sigmoid-sigmoid:  $Y := \sigma(X \cdot \theta_1) \cdot \theta_2 + \sigma(X \cdot \psi_1) \cdot \psi_2 \cdot Z_Y$

where  $Z_Y$  is the ground-truth noise sampled from one of the following distributions: *ContinuousBernoulli*(0.9), *Uniform*(−1, 1), *Exponential*(1), *Beta*(0.5, 0.5), *Gaussian*(0, 1) and *Laplace*(0, 1), and  $\sigma$  is the sigmoid function. Although we did not prove identifiability with *Beta*(0.5, 0.5) noise in Theorem 4.2, empirically we find it is identifiable. Following (Zheng et al., 2018; 2020), each  $\theta$  and  $\psi$  are sampled uniformly from range  $[-2, -0.5] \cup [0.5, 2]$ .  $\phi$  is sampled uniformly from range  $[1, 2]$  to make the *tanh* function positive. The number of data pairs in each synthetic dataset is  $N \in \{500, 5000\}$ .

## H. Hyperparameter Values of CAREFL-H For Table 3b

To acquire the result of CAREFL-H in Table 3b, the hyperparameter values used are as follows:

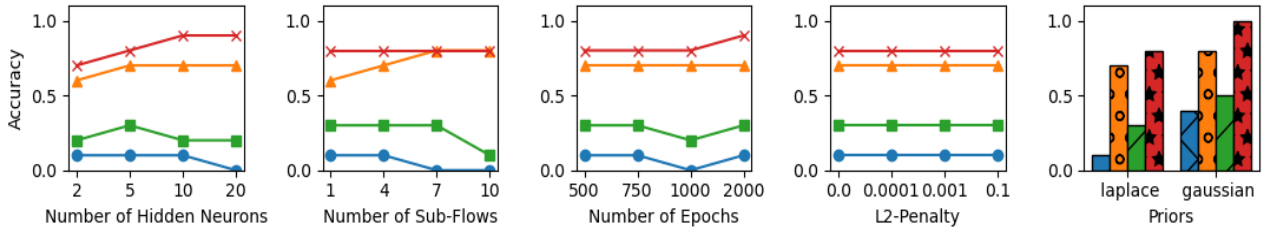
- Number of hidden neurons in each layer of the MLPs: 2
- Number of sub-flows: 10
- Training dataset = testing dataset = 100%.

The rest of the hyperparameter values are identical to the default ones.

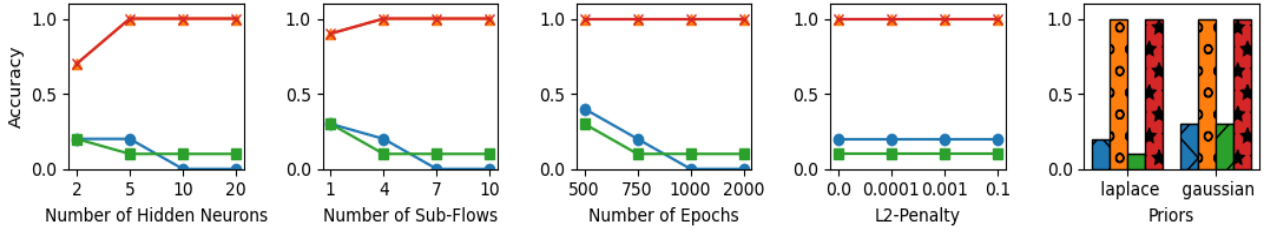
Table 4: (Best viewed in color) Summary of datasets. Settings in Section 6.1 are color-coded. (1) **Blue**: with noise misspecification; (2) **Red**: with more than 50% of datasets having misleading CVs; (3) **Brown**: both (1) and (2).

Type	Name	Noise	$\alpha$	Number of Datasets	Percentage of Datasets With Misleading CVs (%)
Synthetic (Table 1)	LSNM-sine-tanh	<i>Gaussian</i> (0, 1)	0.1	10	30
			0.5	10	50
			1	10	70
			5	10	100
			10	10	100
	LSNM-sine-tanh	<i>Uniform</i> (-1, 1)	0.1	10	30
			0.5	10	90
			1	10	100
			5	10	100
			10	10	100
Synthetic (Section 6.1)	LSNM-tanh-exp-cosine	<i>Uniform</i> (-1, 1)	N/A	10	60
		<i>Beta</i> (0.5, 0.5)		10	80
		<i>ContinuousBernoulli</i> (0.9)		10	70
		<i>Exponential</i> (1)		10	20
		<i>Gaussian</i> (0, 1)		10	40
		<i>Laplace</i> (0, 1)		10	40
	LSNM-sine-tanh	<i>Uniform</i> (-1, 1)	N/A	10	100
		<i>Beta</i> (0.5, 0.5)		10	100
		<i>ContinuousBernoulli</i> (0.9)		10	60
		<i>Exponential</i> (1)		10	20
		<i>Gaussian</i> (0, 1)		10	60
		<i>Laplace</i> (0, 1)		10	80
	LSNM-sigmoid-sigmoid	<i>Uniform</i> (-1, 1)	N/A	10	90
		<i>Beta</i> (0.5, 0.5)		10	100
		<i>ContinuousBernoulli</i> (0.9)		10	80
		<i>Exponential</i> (1)		10	70
		<i>Gaussian</i> (0, 1)		10	90
		<i>Laplace</i> (0, 1)		10	100
Synthetic (Section 6.2)	SIM	N/A	N/A	100	40
	SIM-c			100	46
	SIM-ln			100	23
	SIM-G			100	29
Real-World (Section 6.3)	Tübingen Cause-Effect Pairs	N/A	N/A	99	40

Cause-Effect Inference in Location-Scale Noise Models



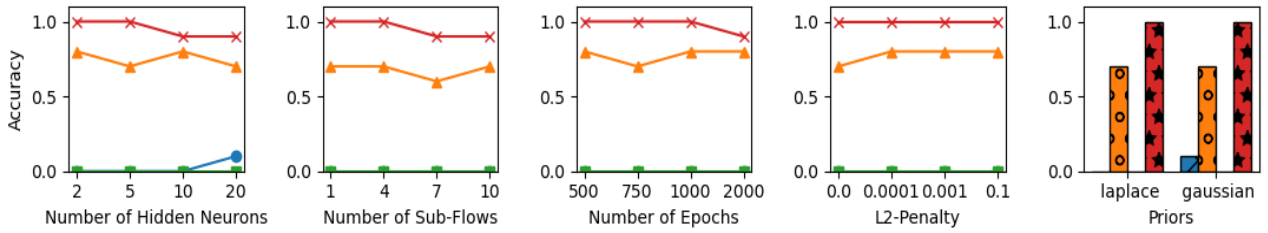
(a)  $N = 500$



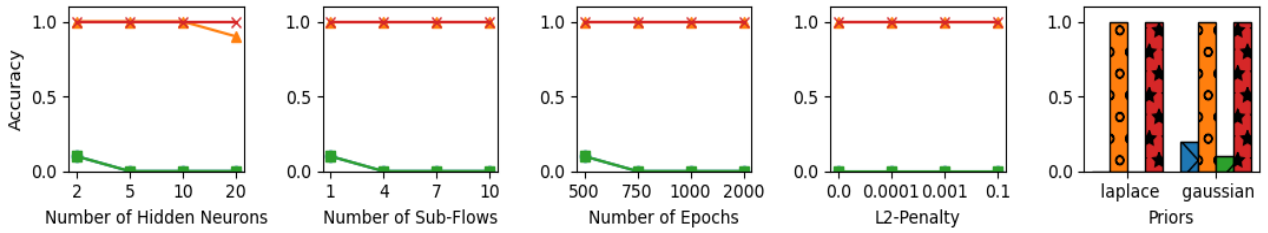
(b)  $N = 5000$



Figure 3: Accuracy over 10 datasets: **LSNM-tanh-exp-cosine** and **Uniform(-1, 1)** noise.



(a)  $N = 500$

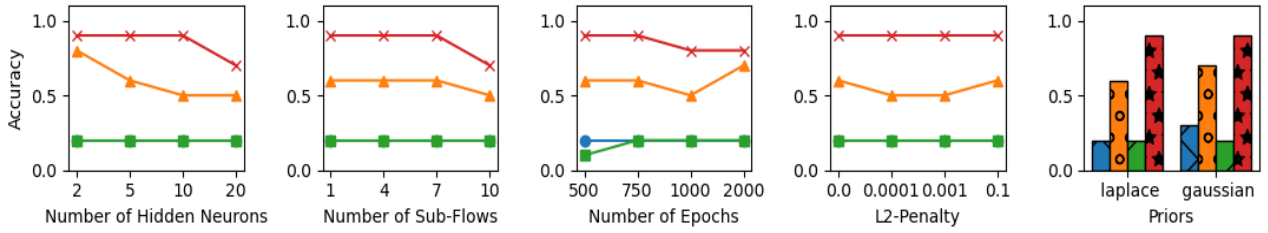


(b)  $N = 5000$

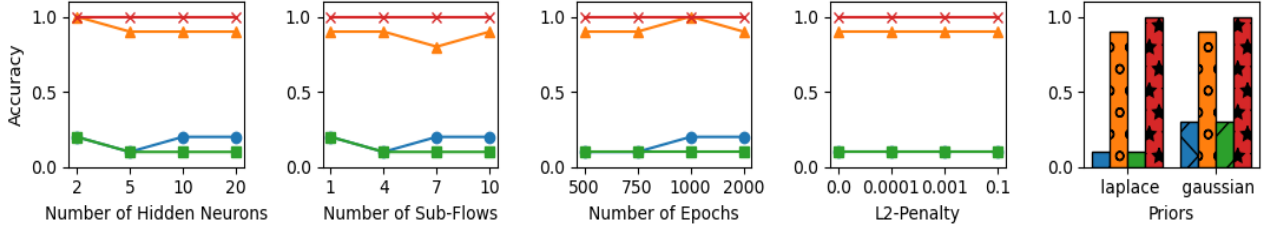


Figure 4: Accuracy over 10 datasets: **LSNM-tanh-exp-cosine** and **Beta(0.5, 0.5)** noise.

Cause-Effect Inference in Location-Scale Noise Models



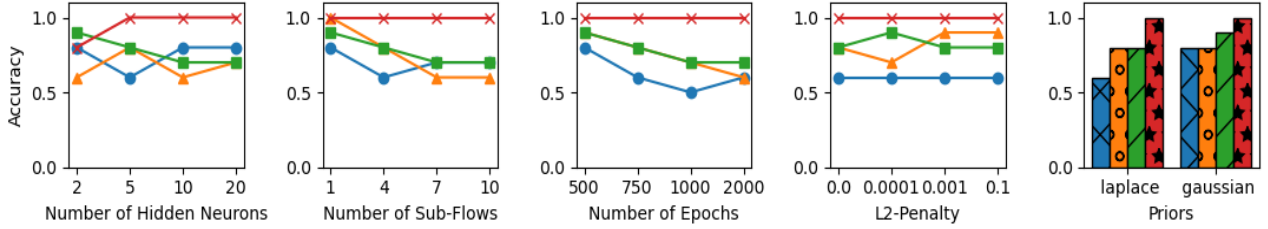
(a)  $N = 500$



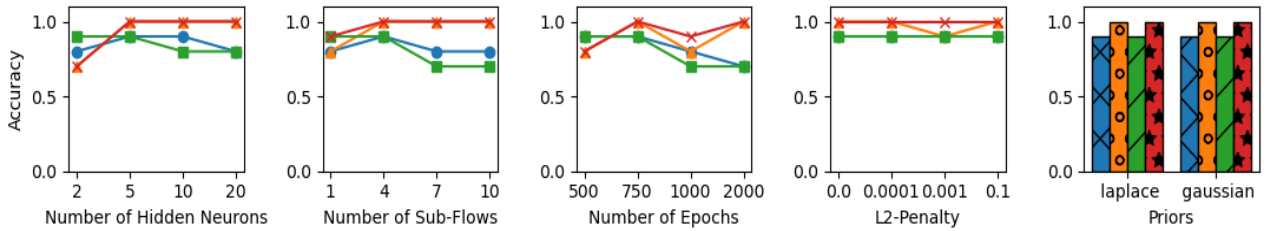
(b)  $N = 5000$



Figure 5: Accuracy over 10 datasets: **LSNM-tanh-exp-cosine** and **ContinuousBernoulli(0.9)** noise.



(a)  $N = 500$

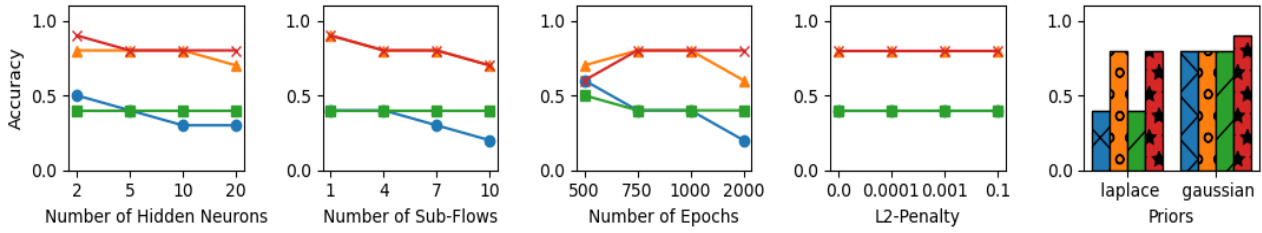


(b)  $N = 5000$

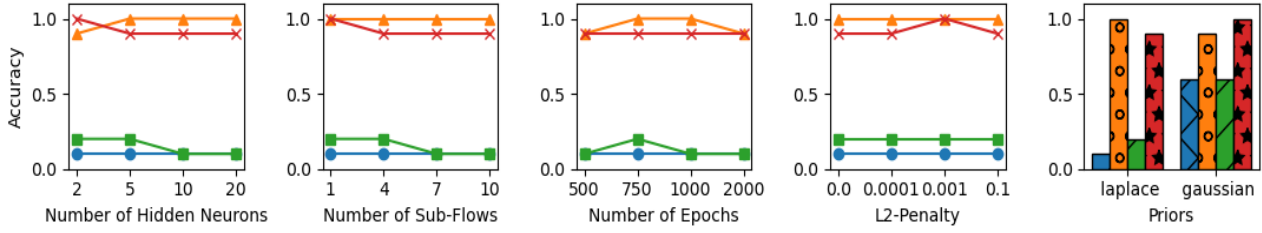


Figure 6: Accuracy over 10 datasets: **LSNM-tanh-exp-cosine** and **Exponential(1)** noise.

Cause-Effect Inference in Location-Scale Noise Models



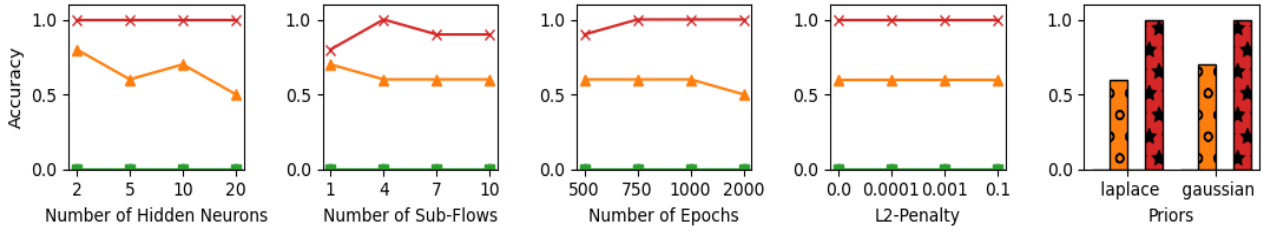
(a)  $N = 500$



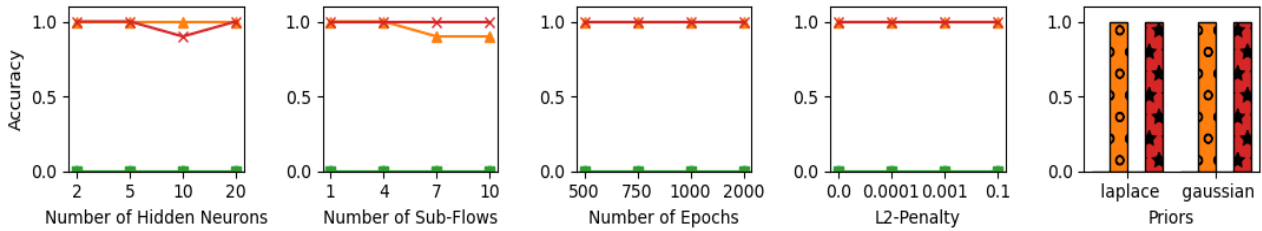
(b)  $N = 5000$



Figure 7: Accuracy over 10 datasets: **LSNM-sine-tanh** and **Uniform(-1, 1)** noise.



(a)  $N = 500$



(b)  $N = 5000$



Figure 8: Accuracy over 10 datasets: **LSNM-sine-tanh** and **Beta(0.5, 0.5)** noise.

Cause-Effect Inference in Location-Scale Noise Models

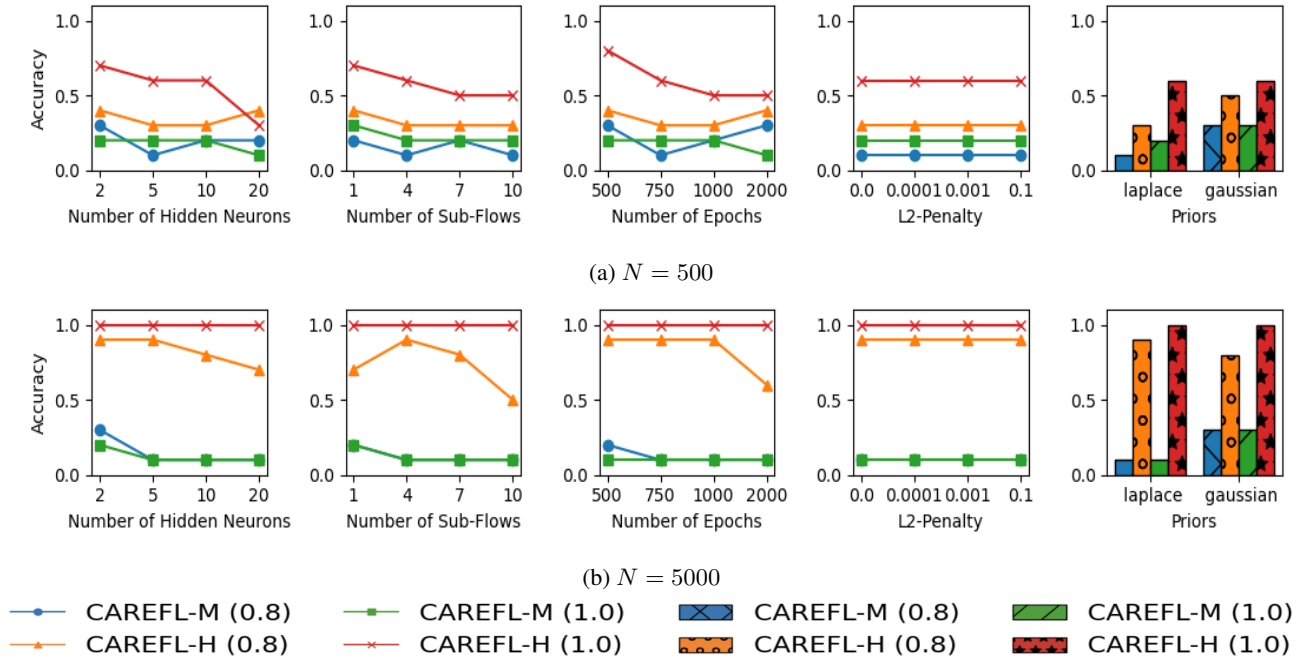


Figure 9: Accuracy over 10 datasets: **LSNM-sine-tanh** and **ContinuousBernoulli(0.9)** noise.

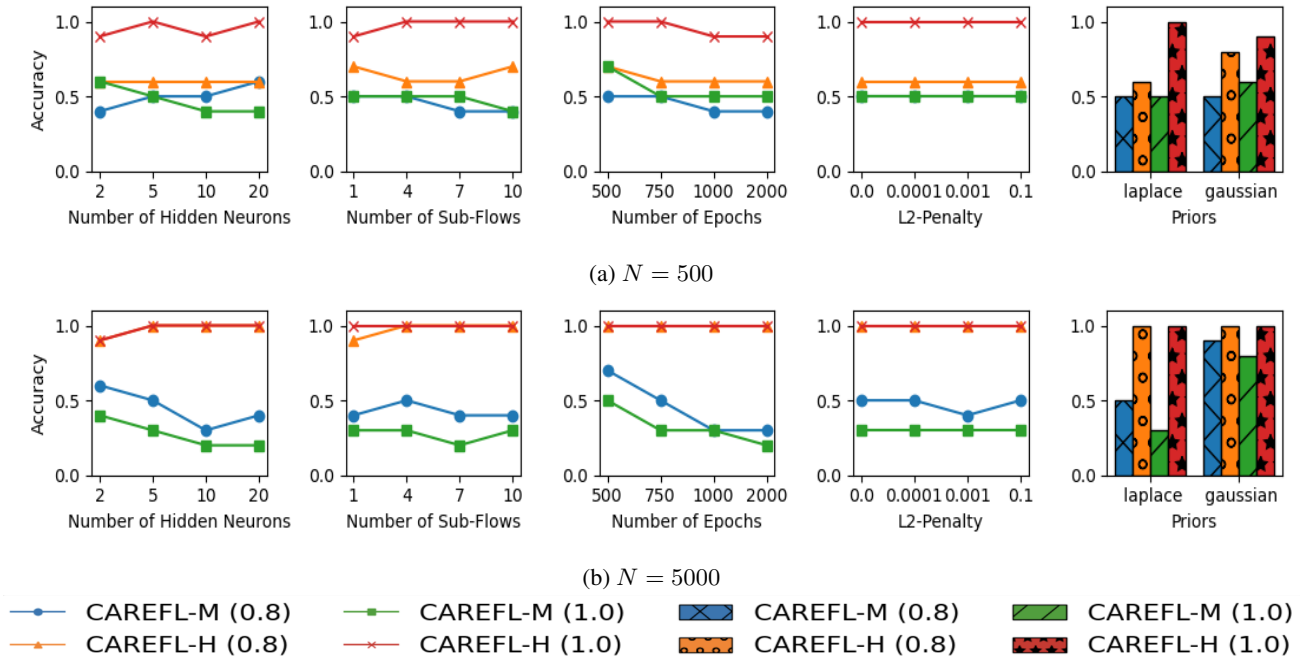
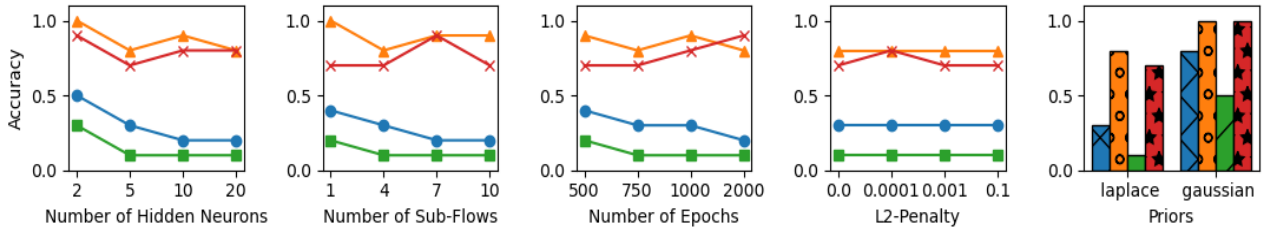
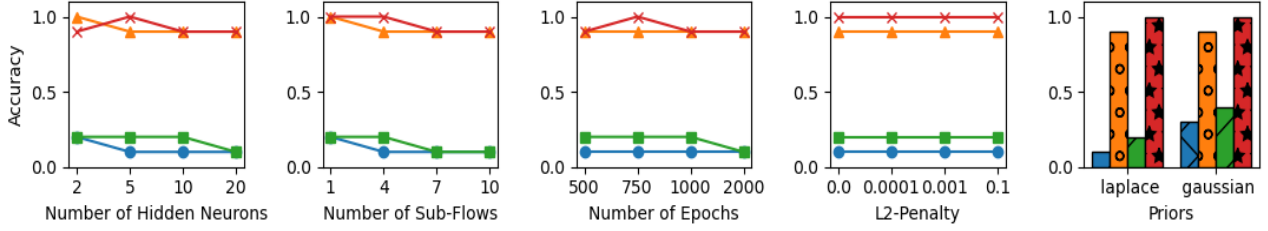


Figure 10: Accuracy over 10 datasets: **LSNM-sine-tanh** and **Exponential(1)** noise.

Cause-Effect Inference in Location-Scale Noise Models



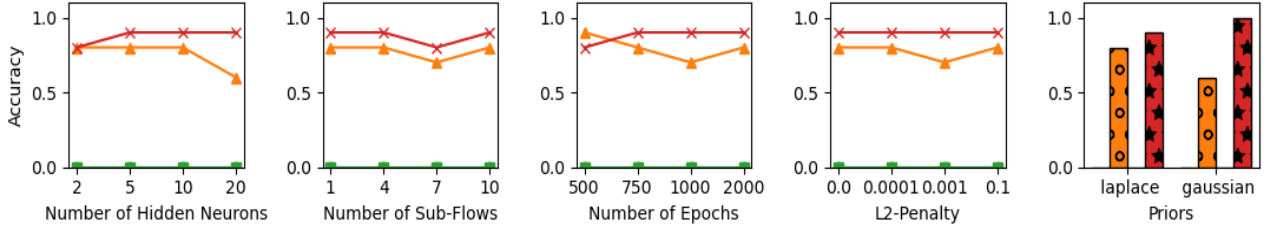
(a)  $N = 500$



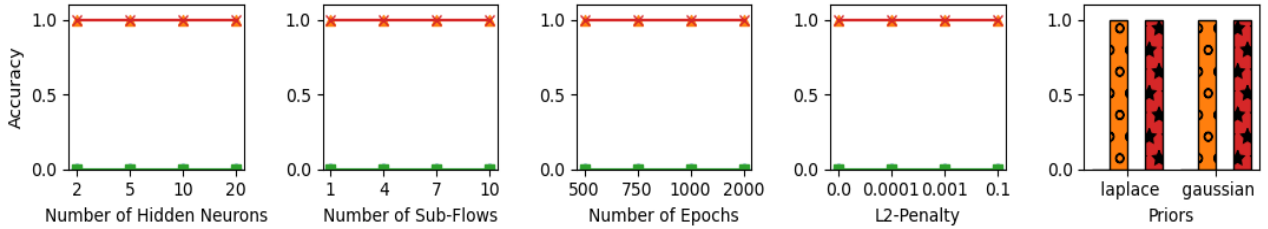
(b)  $N = 5000$



Figure 11: Accuracy over 10 datasets: **LSNM-sigmoid-sigmoid** and **Uniform(-1, 1)** noise.



(a)  $N = 500$

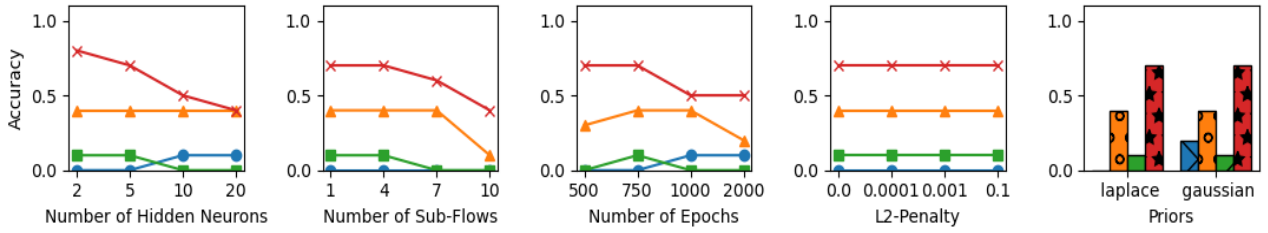


(b)  $N = 5000$

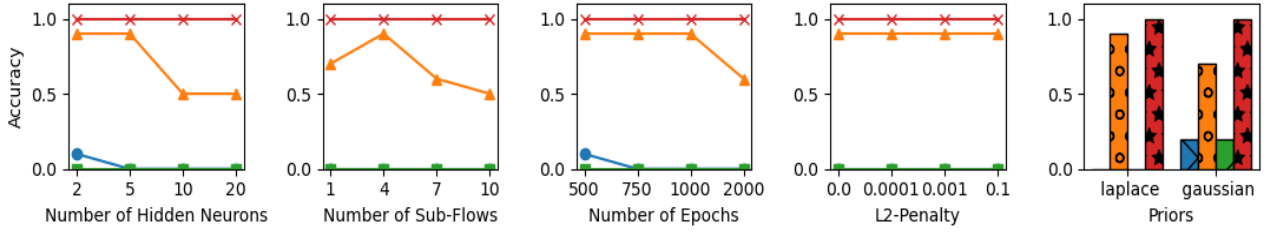


Figure 12: Accuracy over 10 datasets: **LSNM-sigmoid-sigmoid** and **Beta(0.5, 0.5)** noise.

Cause-Effect Inference in Location-Scale Noise Models



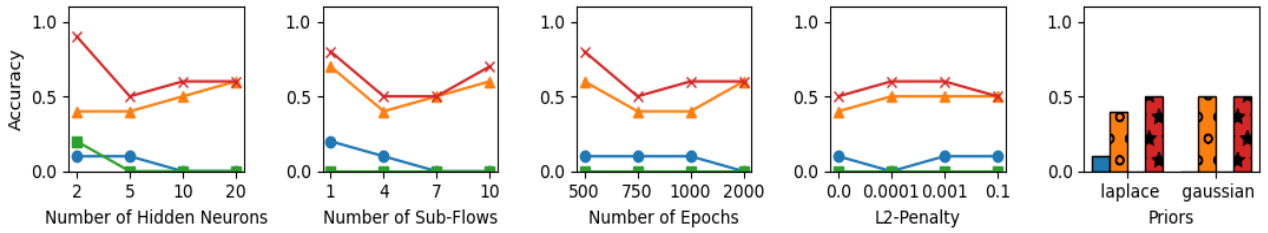
(a)  $N = 500$



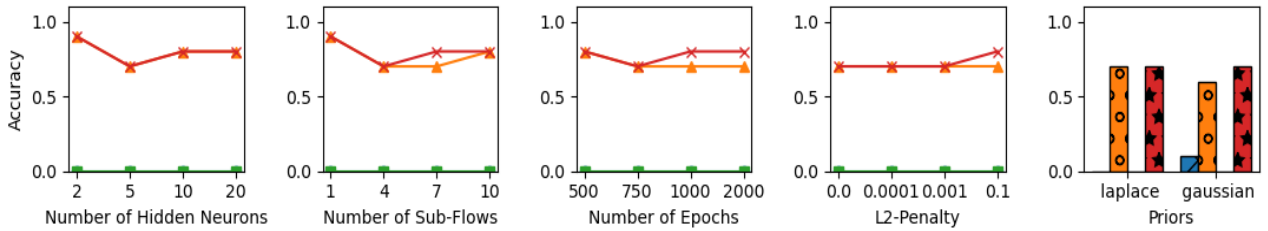
(b)  $N = 5000$



Figure 13: Accuracy over 10 datasets: **LSNM-sigmoid-sigmoid** and **ContinuousBernoulli(0.9)** noise.



(a)  $N = 500$



(b)  $N = 5000$



Figure 14: Accuracy over 10 datasets: **LSNM-sigmoid-sigmoid** and **Exponential(1)** noise.

Cause-Effect Inference in Location-Scale Noise Models

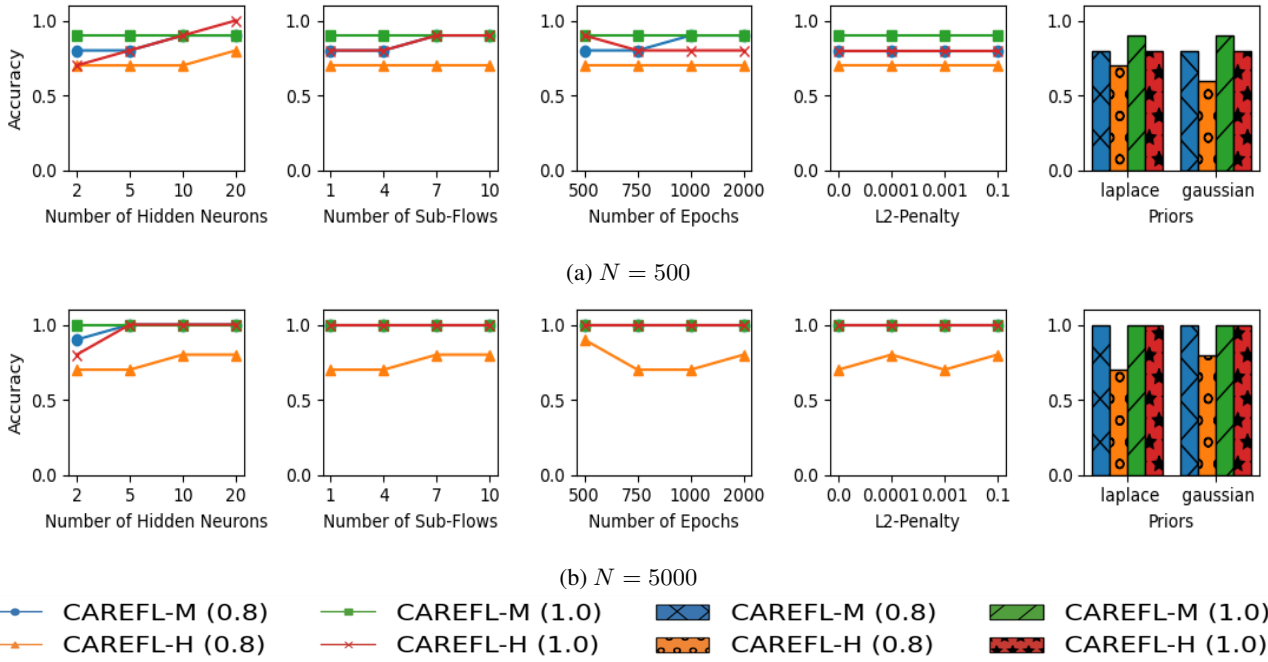


Figure 15: Accuracy over 10 datasets: LSMN-tanh-exp-cosine and Gaussian(0, 1) noise.

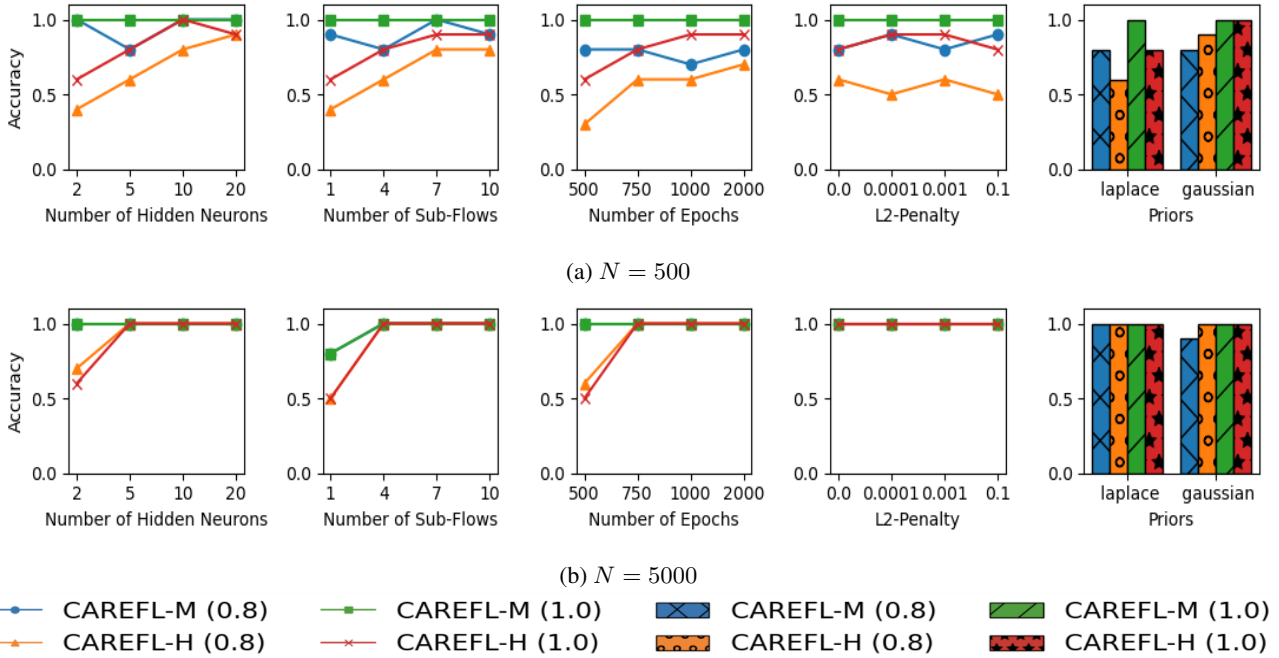
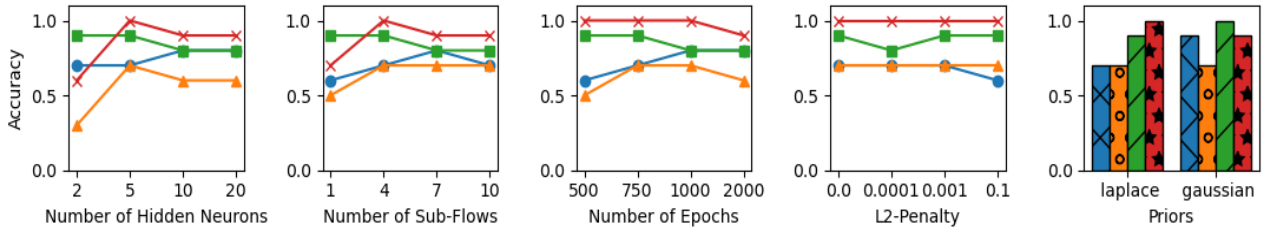
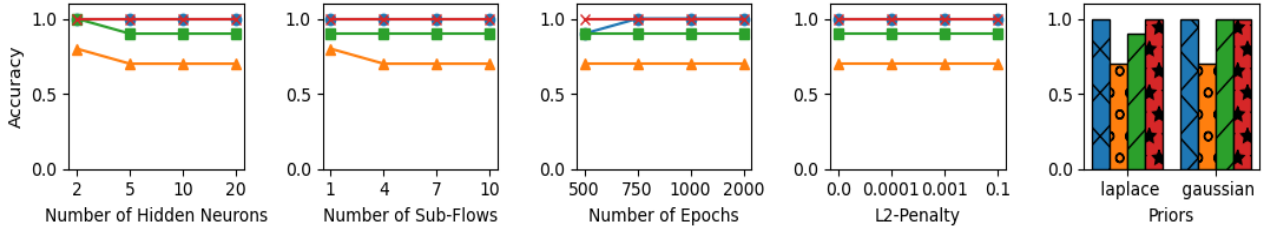


Figure 16: Accuracy over 10 datasets: LSMN-tanh-exp-cosine and Laplace(0, 1) noise.

Cause-Effect Inference in Location-Scale Noise Models



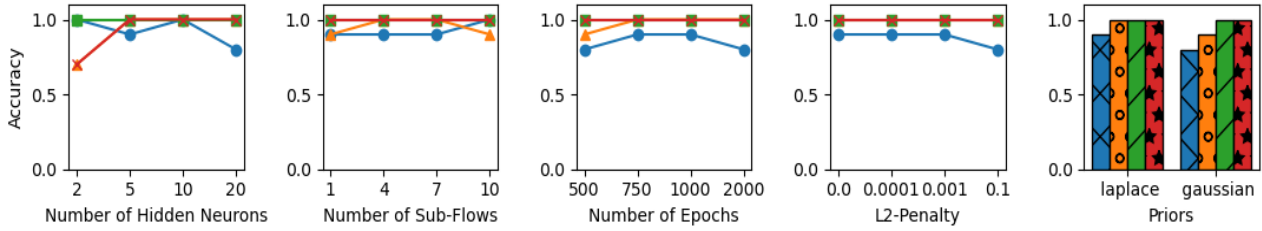
(a)  $N = 500$



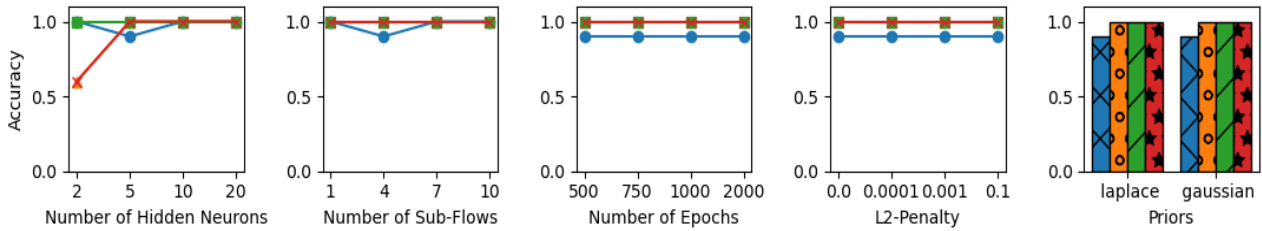
(b)  $N = 5000$



Figure 17: Accuracy over 10 datasets: **LSNM-sine-tanh** and **Gaussian(0, 1)** noise.



(a)  $N = 500$



(b)  $N = 5000$



Figure 18: Accuracy over 10 datasets: **LSNM-sine-tanh** and **Laplace(0, 1)** noise.

Cause-Effect Inference in Location-Scale Noise Models

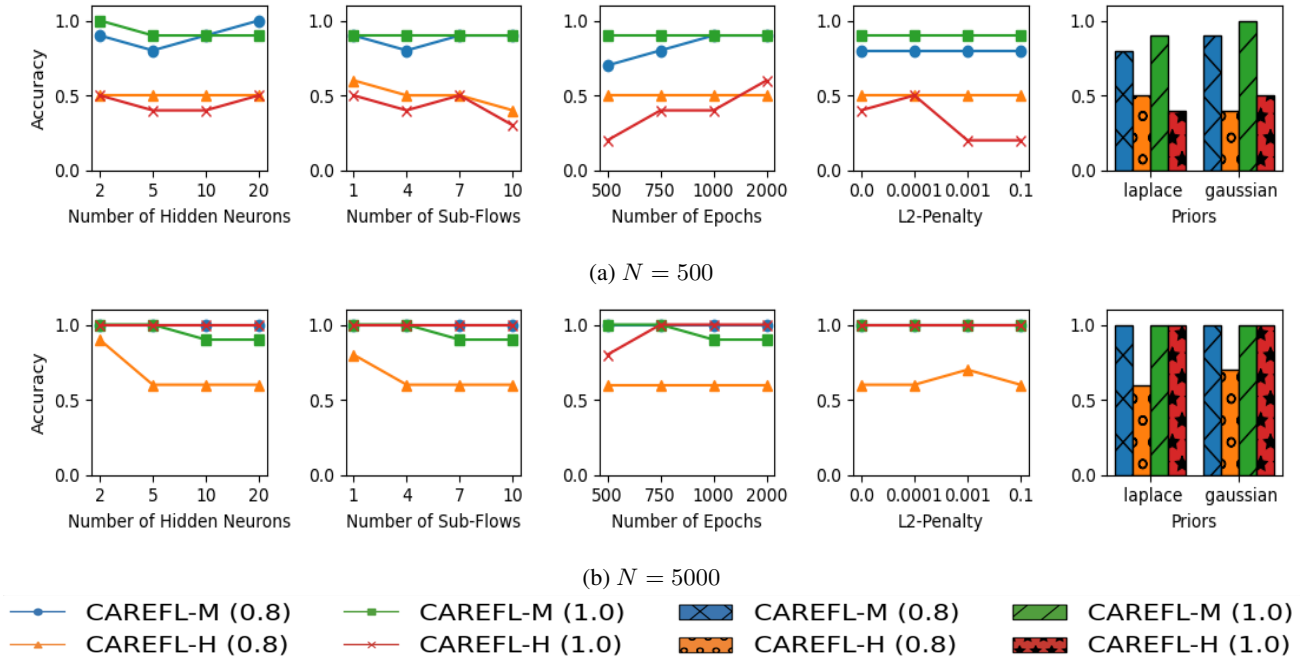


Figure 19: Accuracy over 10 datasets: LSM-sigmoid-sigmoid and Gaussian(0, 1) noise.

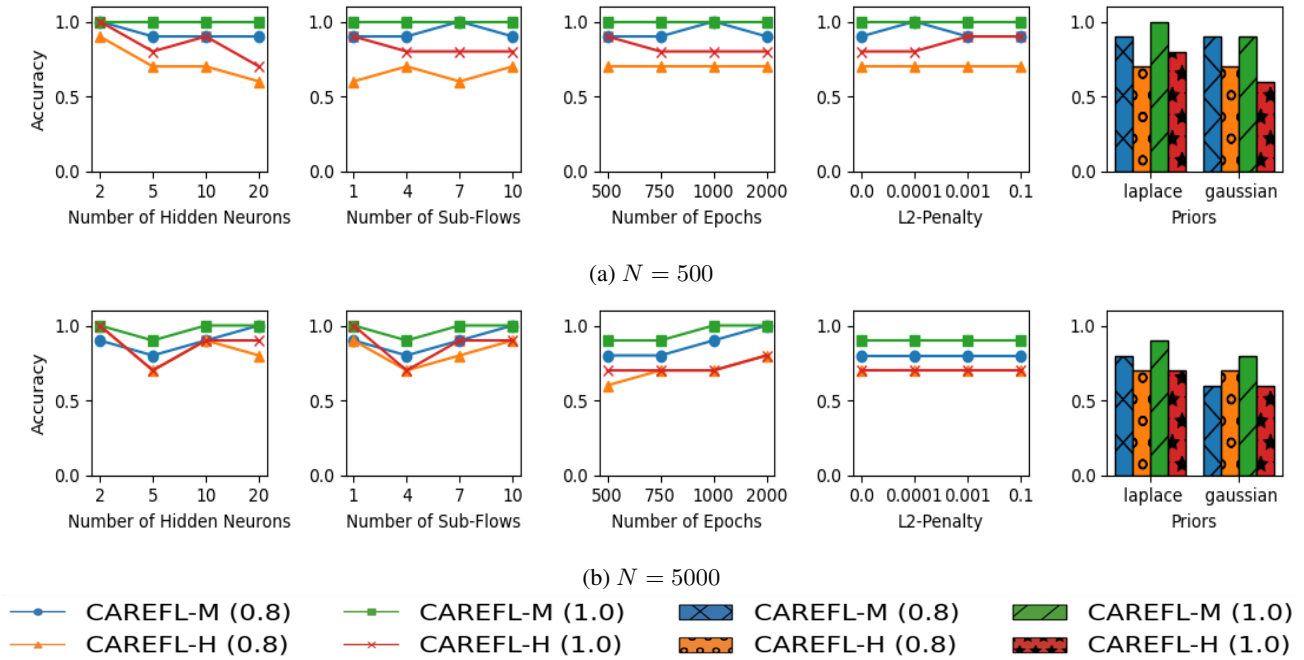


Figure 20: Accuracy over 10 datasets: LSM-sigmoid-sigmoid and Laplace(0, 1) noise.

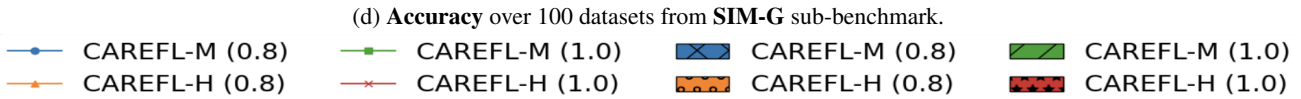
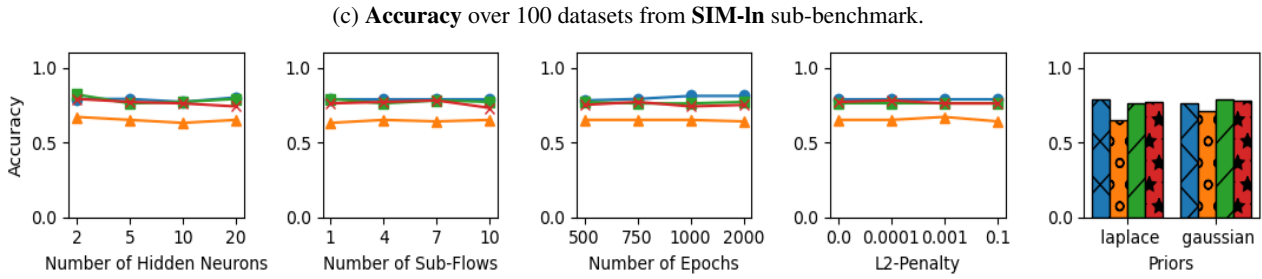
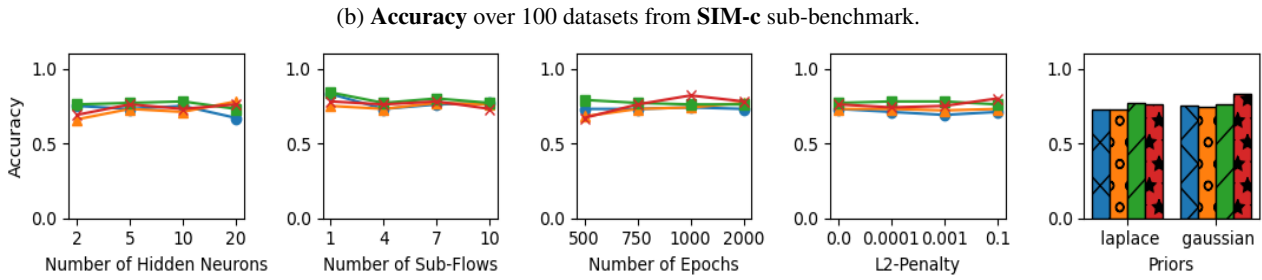
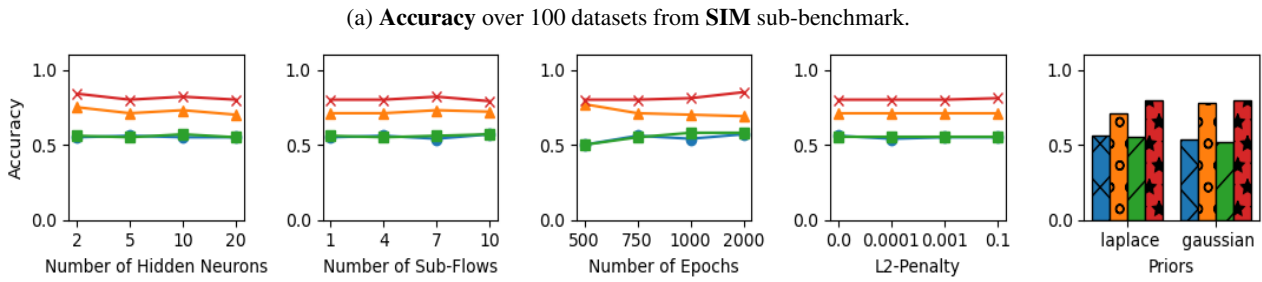
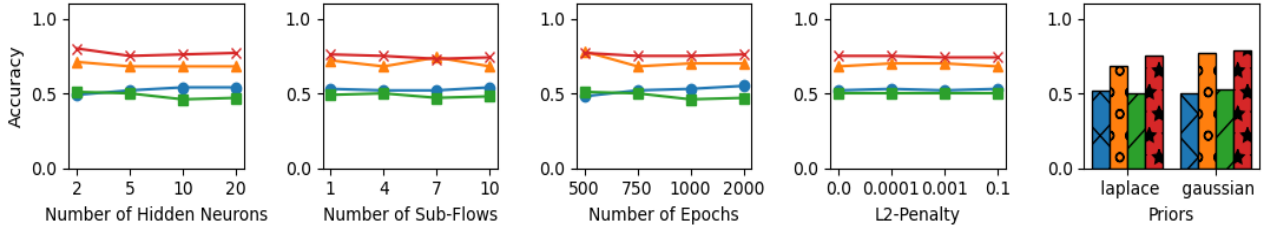


Figure 21: Results with SIM benchmarks.